Part III Essays Easter 2021

E765A

Attach to Front of Essay

Essay Number:

110

Essay Title:

The Search for CMB B-mode Polarization from Inflationary Gravitational Waves

The Search for CMB B-mode Polarization from Inflationary Gravitational Waves

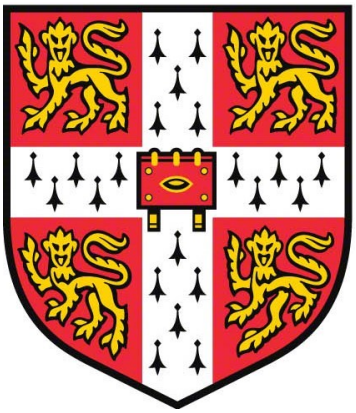

This Essay is submitted as part of the Part III Mathematics Tripos Examination

University of Cambridge, Easter 2021

Contents

1 Introduction

This essay focuses on early-universe cosmology. It explores an aspect of the age-old question "Where do we come from?". In particular, it asks "What mechanism drove the first few moments of the universe, and how can we experimentally test that?". Let us tackle each point in turn.

The present leading paradigm for these initial few moments of the Universe is that of inflation, a period of rapid accelerated expansion of the universe lasting only $\sim 10^{-32}$s. Initially postulated by Guth in 1981 [1] to solve some large conceptual holes in the previous hot Big Bang cosmology, it was soon realized it also provided a convenient method of generating the primordial density fluctuations necessary to seed the growth of large scale structure, setting the 'initial conditions' for the universe.

How do we go about testing inflation? Compared to the complexity of physics on small scales, our cosmic landscape is rather simple. The cosmological principle states that on large scales we expect the universe as a whole to be homogeneous and isotropic. Were this true on all scales, life would not have formed, so it is fortunate this breaks down at some point. These tiny departures from homogeneity are precisely what modern cosmology relies on - they contain vasts amount of information about the universe's evolution. Over the past few decades an era of 'precision cosmology' has been ushered in by ever more accurate measurements of the distribution of mass on cosmic scales through galaxy surveys, and through measurements of the temperature and polarization fluctuations of the cosmic microwave background (CMB). These observables link the late universe to the very early.

The theory community has over the years produced hundreds of well-motivated models for inflation, with data now being required to validate or invalidate any particular one. The simplest, and indeed canonical models of inflation are those of so called single-field slow-roll (SFSR), which generically make a number of predictions validated by increasingly precise measurements of the above observables over the past two decades. Namely the present day spatial flatness of the universe to within 1% and the approximate scale-free, adiabatic, and Gaussian nature of primordial density perturbations. However, there remains more we do not know about inflation than we do; What is the physical mechanism behind it? How and why did it stop? Progress towards these may only be made by putting more stringent observational constraints on the theory space of permissible models. Finally there remains the question as to whether inflation even occurred in the first place - some believe more evidence is needed.

Turning to the subject of this essay, many inflationary models, including the simplest SFSR ones, predict the existence of a stochastic background of primordial inflationary gravitational waves (IGWs), generated through tensor-like quantum-fluctuations of the metric during inflation, which have yet to be detected. Our best strategy for detecting these is through searching for a characteristic 'B mode' polarisation pattern in the CMB. Inflationary scalar (i.e. density) perturbations source CMB temperature anisotropies, as well as an 'E mode' polarisation pattern. Tensor perturbations on the other hand source temperature anisotropies, E mode polarisation and crucially, B mode polarisation too. The B mode diagnostic is therefore our most sensitive test of primordial tensor perturbations - uncontaminated by dominant scalar perturbations.

So far we have made precise measurements of the temperature anisotropy and E mode signal, giving us strong constraints on primordial density perturbations, but have yet to detect these B modes from IGWs. At present, a lack of detection has bounded the 'tensor-to-scalar' ratio r to less than 1 part in 10. A detection of this 'inflationary B mode signal' from IGWs has been termed a 'smoking gun' for inflation as it will provide very strong evidence that inflation did occur, and further will allow us to strongly constrain its physics. A lack of detection of IGWs and therefore r is not useless to us either - it will put more stringent upper bounds on r, invalidating certain classes of models predicting detectably large tensor amplitudes.

1.1 Outline

The structure of this essay is as follows. We begin by reviewing the basics of inflationary cosmology, and a derivation of its predictions in SFSR for the stochastic IGW background. We discuss the parameters commonly used to describe inflationary models and current observational constraints on them. We then turn our attention to the CMB, reviewing the basics of CMB polarisation, and its mathematical description on the curved 2-sphere. We show from the Boltzmann equation formalism that tensor perturbations do indeed produce a non zero B mode signal, and derive their power spectrum, while showing on the other hand that scalar perturbations do not. We then show all is not as easy as it seems, and discuss some major complications in attempting to detect this tiny signal in some detail: the issues of other possible primordial B modes, foregrounds, and gravitational lensing. Finally we return again to inflation, discussing some of the exciting implications a detection of an inflationary B mode signal would have for the cosmology and high energy physics communities.

1.2 Conventions

We use the mostly plus Lorentzian signature $(-,+,+,+)$ in which Greek letters $(\mu,\nu,\ldots)$ are used for spacetime indices, while latin latters $(i,j,\ldots)$ are used for spatial indices. The scale factor is denoted a, and conformal time by τ, which is related to coordinate time by the relation $a(\tau)d\tau = dt$. Coordinate time derivatives are denoted $\dot{}$, and conformal time derivatives $'$, for example the Hubble factor is $H = \frac{\dot{a}}{a}$ and the comoving Hubble factor $\mathcal{H} = \frac{a'}{a}$. We use natural units in which $\hbar = c = k_B = 1$, and where the reduced Planck mass $M_{\rm pl} = 1/\sqrt{8\pi G}$. Our Fourier convention is the inhomogeneous one, where $f(\mathbf{x}) = \int \frac{d^3\mathbf{k}}{(2\pi)^3} f(\mathbf{k}) e^{i\mathbf{k}\cdot\mathbf{x}}$ in 3D, and an analogous statement holds in 2D.

2 Inflationary Cosmology

In this section we review the physics of inflation, and the results relevant for our discussion of CMB observables.

2.1 Inflation Basics

A flat, homogeneous and isotropic universe is described by the Friedmann–Lemaître–Robertson–Walker (FLRW) metric, which in our sign convention takes the form

$$ds^2 = -dt^2 + a^2(t)d\mathbf{x}^2 = a^2(\tau)(-d\tau^2 + d\mathbf{x}^2) \tag{2.1}$$

Assuming General Relativity, it obeys the Einstein equation $G_{ab} = \frac{1}{M_{\rm pl}^2}T_{ab}$, sourced by matter with energy momentum tensor T_{ab}. In cosmological contexts we take this to be a (sum of) perfect fluid(s) with energy momentum tensor satisfying by homogeneity and isotropy

$$T_0^0 = -\rho(t) \quad T_i^0 = 0 \quad T_j^i = P(t)\delta_j^i \tag{2.2}$$

where we identify $\rho(t)$ as the total energy density and $P(t)$ as the total pressure. For the purposes of this section we will consider one component, the inflaton field, to dominate. Substituting 2.1 and 2.2 into the Einstein Equation we obtain the Friedmann equations

$$H^2 = \left(\frac{\dot{a}}{a}\right)^2 = \frac{1}{3M_{\rm pl}^2}\rho \tag{F1}$$

$$\dot{H} + H^2 = \frac{\ddot{a}}{a} = -\frac{1}{6M_{\rm pl}^2}(\rho + 3P) \tag{F2}$$

Inflation requires a shrinking Hubble radius $\frac{d}{dt}\mathcal{H}^{-1} < 0$, equivalent to *accelerated expansion* $\ddot{a} > 0$. We may define the first Hubble slow roll parameter

$$\epsilon := -\frac{\dot{H}}{H^2} = -\frac{d\ln H}{d\ln a} = \frac{3}{2}\left(1 + \frac{P}{\rho}\right) \tag{2.3}$$

where the last equality follows from the Friedmann Equations. We find $\ddot{a} > 0$ is equivalent to $\epsilon < 1$ or to the condition on the equation of state parameter $\omega = P/\rho < -1/3$.

In order to solve the horizon problem we require inflation to persist for a relatively long duration of time ($\sim$ 60 e-folds), so ϵ must remain small. We parametrise how quickly ϵ changes in the second Hubble slow roll parameter

$$\eta = \frac{\dot{\epsilon}}{H\epsilon} = \frac{d\ln\epsilon}{d\ln a} \tag{2.4}$$

which we also require to be small during inflation.

2.1.1 Single Scalar Field Dynamics

The simplest class of inflation models are those consisting of a single effective scalar, the 'inflation' field $\phi(t, \mathbf{x})$, minimally coupled to gravity. The total action is given by

$$S = \int d^4x\sqrt{-g}\left(\frac{M_{\rm pl}^2}{2}R + P(X,\phi)\right) \tag{2.5}$$

for $X = -\frac{1}{2}g^{\mu\nu}\partial_\mu\phi\partial_\nu\phi$. 'Slow roll' inflation corresponds to a canonical kinetic term

$$P(X,\phi) = X - V(\phi) \tag{2.6}$$

where all inflationary dynamics are specified by the potential $V(\phi)$, which the field slowly rolls down. The equations of motion of the classical background $\phi(t)$ may be obtained by directly varying the

action, or making the fluid identification by inserting the energy momentum tensor for the matter Lagrangian into 2.2 and the Friedmann equations F1, F2 giving

$$H^2 = \frac{1}{3M_{\rm pl}^2}\left(\frac{1}{2}\dot{\phi}^2 + V(\phi)\right) \tag{F1'}$$

$$\frac{\ddot{a}}{a} = -\frac{1}{3M_{\rm pl}^2}\left(\dot{\phi}^2 - V(\phi)\right) \tag{F2'}$$

and the Klein Gordon equation

$$\ddot{\phi} + 3H\dot{\phi} = -V' \tag{KG}$$

where $V' = dV/d\phi$. From these we see the spacetime experiences accelerated expansion iff the potential energy dominates the kinetic: $V > \dot{\phi}^2$ and is sustained if $|\ddot{\phi}| \ll |V'|$. We also find by 2.3 that

$$\epsilon = \frac{1}{M_{\rm pl}^2}\frac{\frac{1}{2}\dot{\phi}^2}{H^2} < 1 \tag{2.7}$$

2.1.2 Slow Roll

The slow roll approximation postulates the kinetic energy and acceleration of the background field is much smaller than its potential energy, encapsulated in terms of our slow roll parameters as $(\epsilon, \eta \ll 1)$. In this approximation F1' and KG become

$$\begin{aligned} H^2 &\approx \frac{V}{3M_{\rm pl}^2} \\ 3H\dot{\phi} &\approx -V' \end{aligned} \tag{2.8}$$

from which we see

$$\epsilon \approx \frac{1}{2}M_{\rm pl}^2\left(\frac{V'}{V}\right)^2 =: \epsilon_V \tag{2.9}$$

where we have defined the first *potential* slow roll parameter. We can analogously define a second potential slow roll parameter via

$$\eta_V = M_{\rm pl}^2\frac{V''}{V} \approx 2\epsilon - \frac{1}{2}\eta \tag{2.10}$$

which must therefore also be small. With these constraints satisfied, inflation occurs and inflates the universe in a quasi-de Sitter fashion

$$a(t) \approx a(0)e^{Ht} \qquad H \approx \text{constant} \tag{2.11}$$

Since ϕ acts as a clock during inflation, we may express the number of e-folds of inflation from a time t until the end of inflation as an integral over field excursion instead of time

$$N(t) := \ln\frac{a(t_{end})}{a(t)} = \int_a^{a(t)} d(\ln a) = \int_t^{t_{end}} H dt = \int_{\phi(t)}^{\phi_{end}} \frac{d\phi}{\sqrt{2\epsilon}M_{\rm pl}} \tag{2.12}$$

using $Hdt = \frac{H}{\dot{\phi}}d\phi = \frac{d\phi}{\sqrt{2\epsilon}M_{\rm pl}}$

2.2 Cosmological Perturbation Theory

So far we have only considered the homogeneous and isotropic background for the inflaton. In general it can also vary in space, as can the metric, which also experiences perturbations following [2].

$$\phi(t,\mathbf{x}) = \bar{\phi}(t) + \delta\phi(t,\mathbf{x}) \qquad g_{\mu\nu}(t,\mathbf{x}) = \bar{g}_{\mu\nu}(t,\mathbf{x}) + \delta g_{\mu\nu}(t,\mathbf{x}) \tag{2.13}$$

As ever, we adapt our variables to the symmetries of the problem at hand. Spatial translations are diagonalized by working in Fourier space, where distinct Fourier modes decouple at linear order. Rotations can be separated into (rotation) scalars, vectors and tensors, with 0, 1 and 2 spatial indices. The Scalar-Vector-Tensor decomposition gives

$$\begin{aligned} ds^2 &= g_{\mu\nu}dx^\mu dx^\nu \\ &= -(1+2\Phi)dt^2 + 2aB_i dx^i dt + a^2[(1-2\Psi)\delta_{ij} + E_{ij}]dx^i dx^j \end{aligned} \tag{2.14}$$

$$\begin{aligned} B_i &= \partial_i B - B_i, \quad \partial^i B_i = 0 \\ E_{ij} &= 2\partial_{ij}E + 2\partial_{(i}E_{j)} + h_{ij}, \quad \partial^i E_i = 0, \quad h^i_i = \partial^i h_{ij} = 0 \end{aligned} \tag{2.15}$$

Crucially, at linear order scalars, vectors and tensors evolve independently, and so can be treated separately. Importantly the perturbations $\delta\phi$ and $\delta g_{\mu\nu}$ are gauge dependent variables, and mix the scalars, vectors and tensors separately under coordinate transformations. We therefore must either work in a fixed gauge or use gauge invariant quantities.

Scalars - An important gauge invariant quantity is the comoving curvature perturbation, given at linear order by

$$-\zeta = \Psi + \frac{H}{\dot{\rho}}\delta\rho \tag{2.16}$$

for ρ the total energy density of the universe. Note often ζ is denoted $\mathcal{R}$. During inflation, and in comoving gauge where $\delta\rho_\phi = 0$ all dynamical scalar degrees of freedom (the others obey constraint equations) can be expressed by a single metric perturbation

$$g_{ij} = a^2(t)[1+2\zeta]\delta_{ij} \tag{2.17}$$

so ζ describes spatial curvature: the 3 dimensional Ricci scalar of these constant density hypersurfaces is given by $\mathcal{R}^{(3)} = -4\nabla^2\zeta/a^2$. It turns out ζ is the adiabatic mode that 'freezes out' outside the horizon [3, 4]. This is important since during inflation modes eventually exit the horizon, re-entering at a time after inflation ends and the horizon has grown again. Being gauge invariant, we may compute it in any gauge - in the spatially flat gauge $\Psi = 0$, so ζ is simply the dimensionless density perturbation. One can construct transfer functions relating the late time evolved values of cosmological fields to this initial frozen value of ζ.

Thus ζ is the relevant quantity describing primordial scalar perturbations. Its dimensionless power spectrum is given by

$$\langle\zeta(\mathbf{k})\zeta(\mathbf{k}')\rangle = (2\pi)^3\delta(\mathbf{k}+\mathbf{k}')\frac{2\pi^2}{k^3}\Delta^2_s(k) \tag{2.18}$$

with scale dependence described by the scalar spectral index

$$n_s - 1 = \frac{d\ln\Delta^2_s}{d\ln k} \tag{2.19}$$

giving the approximate form

$$\Delta^2_s(k) \approx A_s(k_*)\left(\frac{k}{k_*}\right)^{n_s-1} \tag{2.20}$$

where k_* is some pivot scale.

Vectors - It can be shown vectors decay rapidly as the universe expands, and may be neglected as they are not expected to contribute significantly to the relevant CMB observables if generated during inflation. There are exceptions to this, see section 4.1.

Tensors - Since there is only one tensor h_{ij}, and coordinate transformations don't introduce tensors, it must be gauge invariant to linear order. This term is in essence responsible for the content of the

rest of the essay - it describes IGWs, which are also adiabatic and freeze out on superhorizon scales. The relevant quantity to consider is again its power spectrum

$$\langle h_{ij}(\mathbf{k}) h_{ij}(\mathbf{k}') \rangle = (2\pi)^3 \delta(\mathbf{k}+\mathbf{k}') \frac{2\pi^2}{k^3} \Delta_t^2(k) \tag{2.21}$$

with scale dependence defined analogously as

$$n_t = \frac{d \ln \Delta_t^2}{d \ln k} \tag{2.22}$$

giving the approximate form

$$\Delta_t^2(k) \approx A_t(k_*) \left(\frac{k}{k_*} \right)^{n_t} \tag{2.23}$$

We can now define the important parameter r, the tensor to scalar ratio

$$r(k_*) = \frac{A_t(k_*)}{A_s(k_*)} \tag{2.24}$$

2.3 SFSR Power Spectra

The scalar and tensor power spectra are model dependent. We compute them in the SFSR regime in Appendix A, with key results being

$$\Delta_s^2(k) = \frac{1}{2\epsilon M_{\rm pl}^2} \left(\frac{H}{2\pi} \right)^2 |_{k=aH} \qquad \Delta_t^2(k) = \frac{2}{\pi^2} \left(\frac{H}{M_{\rm pl}} \right)^2 |_{k=aH} \tag{2.25}$$

These power spectra provide the initial conditions of the universe. Given a good understanding of the physics of proceeding cosmological evolution we have several direct probes of them. Later sections of this essay will go into more detail about signatures of the tensor power spectrum in particular.

Here we investigate some of their properties. Recall H is approximately constant during inflation, but not perfectly so, since $H^2 \sim V(\phi)$, and ϕ is slowly rolling down its potential. Similarly ϵ also varies slightly, and so we expect slight deviations from scale invariance: $n_s - 1 \approx 0$, $n_t \approx 0$. We can compute the spectral indices in terms of the slow roll parameters.

$$\begin{aligned} n_s - 1 &= \frac{d \ln \Delta_s^2}{d \ln k} = \frac{d}{d \ln k} (2 \ln H - \ln \epsilon) \approx \frac{1}{H} \frac{d}{dt} (2 \ln H - \ln \epsilon) = \frac{2\dot{H}}{H^2} - \frac{\dot{\epsilon}}{H\epsilon} \\ &= -2\epsilon - \eta = -6\epsilon_V + 2\eta_V \\ n_t &= \frac{d \ln \Delta_t^2}{d \ln k} = \frac{d}{d \ln k} 2 \ln H \\ &= -2\epsilon = -2\epsilon_V \end{aligned} \tag{2.26}$$

where we have used that $d \ln k = d \ln aH \approx d \ln a = H dt$ since we evaluate the power spectra at horizon exit, and H is slowly varying (so $d \ln H$ provides a next to leading order correction). During inflation $\epsilon > 0$ since energy density is monotonically decreasing, and so $n_t < 0$ and tensor perturbations are said to have a red spectrum. n_s on the other hand can have either a red ($n_s < 1$) or blue ($n_s > 1$) spectrum. The scalar to tensor ratio can be computed as

$$r = \frac{A_t}{A_s} \approx 16\epsilon \tag{2.27}$$

giving the consistency condition $r = -8 n_t$, which serves as a test, at least in principle, of SFSR.

2.4 Current Observational Constraints

A number of inflationary parameters have been measured through CMB experiments. From Planck 2018 temperatuere, polarisation and lensing data at 68% confidence and for the purposes of this essay, the relevant parameters include [5]

- A red tilted scalar spectral index $n_s = 0.9649 \pm 0.0042$, with no evidence for scale dependence of n_s. The perfectly scale invariant $n_s = 1$ spectrum is ruled out by more than 8σ, providing strong evidence for inflation.
- A scalar amplitude $10^9 A_s \approx 2.100 \pm 0.030$.

We have not yet made a detection of any primordial tensor perturbations, and only have a 95% confidence upper limit on the tensor to scalar ratio $r_{0.002} < 0.10$ from Planck data alone, or $r_{0.002} < 0.056$ by also making use of the BICEP2/Keck Array BK15 data [6], where the subscripts denote the pivot scale. We obviously have no bounds on n_t.

In order to get a better understanding of the physics of inflation, we would really like to get a better constraint on r initially, and n_t in future. We explore the physics implications of these parameters later in section 5, though we first must explain how on earth we are going to measure them.

3 The B Mode Diagnostic

We now turn to how we go about measuring r. The CMB contains vasts amount of information within its small temperature (T) anisotropies, but also turns out to be partially polarised, encoding further, harder to extract, information. While Thomson scattering of isotropic radiation would produce no polarisation, the CMB possesses a quadrupolar (Y_{2m}) temperature variation, which gives rise to linear polarisation upon scattering. When Thomson scattering is rapid, the randomization of photon directions destroys this quadrupole anisotropy and therefore polarization. So, the problem of understanding the polarization pattern of the CMB reduces to understanding the quadrupolar temperature fluctuations when the rate has suffiecently slowed, i.e. at last scattering [7], though note reionization also contributes some polarisation. Polarisation is a more direct probe of these epochs than temperature, unaffected by later universe 'integrated' effects such as the integrated Sachs-Wolfe effect. In this section we first introduce the formalism in which we may define polarisation fields on the full sky, then compute using the 'line of sight' method the angular power spectrum of B modes arising from IGWs, which we find to be non zero. In contrast we show scalar perturbations don't produce any B modes, instead only contributing to the T and E power spectra. Thus, a measurement of a non zero B mode signal gives us a direct probe of the primordial tensor power spectrum, and, combining with the primordial scalar power spectrum, r.

3.1 CMB Observables

A CMB Photon detector measures the electric field $\mathbf{E}$ perpendicular to the direction of observation $\hat{\mathbf{n}}$, from which we can define a rank two intensity correlation tensor following for example [8, 9].

$$I_{ij} = \langle E_a E_b^* \rangle \tag{3.1}$$

where $\langle\rangle$ denotes a time average over several periods over which the amplitude changes insignificantly. Rank two tensors can be decomposed into three irreducible components: a trace part, a symmetric trace free part, and an antisymmetric part. Fixing an orthonormal basis $\{\hat{\mathbf{e}}_1, \hat{\mathbf{e}}_2\}$ orthogonal to the line of sight $\hat{\mathbf{n}}$ we encode the four degrees of freedom as

$$I_{ij} = \frac{1}{2}\begin{pmatrix} I+Q & U+iV \\ U-iV & I-Q \end{pmatrix} \tag{3.2}$$

The antisymmetric part encodes a phase lag between E_1 and E_2, i.e. circular polarization V. Thomson scattering induces no such polarisation and so we may neglect this [10]. The polarisation matrix is therefore

$$P_{ij} = \frac{1}{2}\begin{pmatrix} Q & U \\ U & -Q \end{pmatrix} \tag{3.3}$$

Q and U are standard Stokes' parameters, which are functions of frequency and direction in general. In linear theory, their frequency dependence follows that of temperature anisotropies. We therefore normalize Q and U with respect to temperature rather than intensity, by dividing by the derivative of the CMB blackbody brightness with respect to log temperature, obtaining frequency independent fractional thermodynamic equivalent temperatures $Q(\hat{\mathbf{n}})$ and $U(\hat{\mathbf{n}})$ [11].

The Q parameter can be thought of as the difference in power measured between an observer aligned with $\hat{\mathbf{e}}_1$ and $\hat{\mathbf{e}}_2$ while U can be thought of as the difference between $\hat{\mathbf{e}}_1 \pm \hat{\mathbf{e}}_2$. Note P_{ij} has eigenvalues $\pm(Q^2+U^2)^{\frac{1}{2}}$, with magnitude the polarisation amplitude, and corresponding eigenvectors making an angle of $\frac{1}{2}\arctan(\frac{U}{Q})$ with $\hat{\mathbf{e}}_1$. Diagrammatically, we may therefore depict polarisation as headless vectors of length $(Q^2+U^2)^{\frac{1}{2}}$, making an angle of $\frac{1}{2}\arctan(\frac{U}{Q})$ to $\hat{\mathbf{e}}_1$, so that the direction indicates the axis of measurement maximising measured signal.

Since δ_{ij} is the unique symmetric tensor invariant under rotations we see that I is invariant under rotations, but Q and U are not. In particular if we perform a right handed rotation around $\hat{\mathbf{n}}$ by an

angle ψ we get transformations

$$\begin{pmatrix} \hat{\mathbf{e}}_1' \\ \hat{\mathbf{e}}_2' \end{pmatrix} = \begin{pmatrix} \cos\psi & \sin\psi \\ -\sin\psi & \cos\psi \end{pmatrix} \begin{pmatrix} \hat{\mathbf{e}}_1 \\ \hat{\mathbf{e}}_2 \end{pmatrix} \tag{3.4}$$

$$\begin{pmatrix} Q' \\ U' \end{pmatrix} = \begin{pmatrix} \cos 2\psi & \sin 2\psi \\ -\sin 2\psi & \cos 2\psi \end{pmatrix} \begin{pmatrix} Q \\ U \end{pmatrix} \tag{3.5}$$

The fact that Q and U are basis dependent is a nuisance: they aren't physical, and cannot be compared meaningfully at different points on the sphere. The polarisation tensors live in different vector spaces: entirely analogous with the same concept in differential geometry.

It is convenient to instead work with complex quantities $Q \pm iU$, equivalent to working in the complex basis $\hat{\mathbf{e}}_\pm = \frac{1}{\sqrt{2}}(\hat{\mathbf{e}}_1 \pm i\hat{\mathbf{e}}_2)$ in which the polarisation tensor is diagonal. Using 3.5, it is easy to see under rotation these quantities transforms more simply as

$$Q' \pm iU' = e^{\mp 2i\psi}(Q \pm iU) \tag{3.6}$$

Now a definition: A function $f(\theta, \phi)$ on the sphere is said to have *spin* s if under a right handed rotation by angle ψ of orthogonal vectors $(\hat{\mathbf{e}}_1, \hat{\mathbf{e}}_2)$ tangential to the sphere, it transforms as $f'(\theta, \phi) = e^{-is\psi} f(\theta, \phi)$. A spin 0 quantity is therefore a scalar under rotations. Note these rotations are not of the sphere, but instead of the tangent space orthogonal to $\hat{\mathbf{n}}$.

Thus $Q + iU$ is a spin 2 quantity, $Q - iU$ a spin -2 quantity, and T a spin 0 quantity. From here on out we use the natural choice of tangential basis at a point along line of sight $\hat{\mathbf{n}} = \hat{\mathbf{n}}(\theta, \phi)$ on the sphere: $(\hat{\mathbf{e}}_1, \hat{\mathbf{e}}_2) = (\hat{\mathbf{e}}_\theta, \hat{\mathbf{e}}_\phi)$. Apart from the neater transformation law, the main reason we construct these quantities of definite spin is that analogously to the expansion of scalar quantities in terms of spherical harmonics

$$T(\hat{\mathbf{n}}) = \sum_{lm} T_{lm} Y_{lm}(\hat{\mathbf{n}}) \tag{3.7}$$

there also exist 'spin weighted spherical harmonics' ${}_sY_{lm}$ forming a complete orthonormal basis for spin s weighted functions [12]. Properties of these functions, and their relation to standard spherical harmonics are listed in Appendix B. In terms of these we may expand

$$(Q \pm iU)(\hat{\mathbf{n}}) = \sum_{lm} a_{\pm 2,lm} {}_{\pm 2}Y_{lm}(\hat{\mathbf{n}}) \tag{3.8}$$

By reality conditions on T, Q and U we have

$$T^*_{lm} = T_{l,-m} \qquad a^*_{-2lm} = a_{2lm} \tag{3.9}$$

We now solve our problem of coordinate dependence of Q and U by introducing spin raising ($\eth$) and lowering ($\bar{\eth}$) operators, which raise or lower the spin weight of a function by 1. Their properties, and explicit forms may be found in Appendix B. We construct two rotationally invariant scalar quantities out of $Q \pm iU$ by acting twice on 3.8 with our raising and lowering operators

$$\begin{aligned} \eth^2(Q - iU)(\hat{\mathbf{n}}) &= \sum_{lm} \left[\frac{(l+2)!}{(l-2)!}\right]^{1/2} a_{2,lm} Y_{lm}(\hat{\mathbf{n}}) \\ \bar{\eth}^2(Q + iU)(\hat{\mathbf{n}}) &= \sum_{lm} \left[\frac{(l+2)!}{(l-2)!}\right]^{1/2} a_{-2,lm} Y_{lm}(\hat{\mathbf{n}}) \end{aligned} \tag{3.10}$$

where now we can express $a_{\pm 2,lm}$ using orthogonality of (spin weighted) spherical harmonics

$$\begin{aligned} a_{2,lm} &= \int d\Omega_2 Y^*_{lm}(\hat{\mathbf{n}})(Q+iU)(\hat{\mathbf{n}}) \\ &= \left[\frac{(l+2)!}{(l-2)!}\right]^{-1/2} \int d\Omega Y^*_{lm}(\hat{\mathbf{n}})\bar{\eth}^2(Q+iU)(\hat{\mathbf{n}}) \\ a_{-2,lm} &= \int d\Omega_2 Y^*_{lm}(\hat{\mathbf{n}})(Q-iU)(\hat{\mathbf{n}}) \\ &= \left[\frac{(l+2)!}{(l-2)!}\right]^{-1/2} \int d\Omega Y^*_{lm}(\hat{\mathbf{n}})\eth^2(Q-iU)(\hat{\mathbf{n}}) \end{aligned} \tag{3.11}$$

We construct two linear combinations of these modes, the physical E and B modes. The sign choice here is non universal and follows that of [12], though for the purposes of calculating power spectra the choice does not matter.

$$\begin{aligned} E_{lm} &= -(a_{2,lm} + a_{-2,lm})/2 \\ B_{lm} &= i(a_{2,lm} - a_{-2,lm})/2 \end{aligned} \tag{3.12}$$

Using these we may rewrite 3.8 as

$$(Q \pm iU)(\hat{\mathbf{n}}) = -\sum_{lm}(E_{lm} \pm iB_{lm})_{\pm 2}Y_{lm}(\hat{\mathbf{n}}) \tag{3.13}$$

For real space calculations we introduce related quantities, which are manifestly rotationally invariant

$$\begin{aligned} \tilde{E}(\hat{\mathbf{n}}) &:= -\frac{1}{2}[\bar{\eth}^2(Q+iU) + \eth^2(Q-iU)] \\ &= \sum_{lm} \tilde{E}_{lm}Y_{lm}(\hat{\mathbf{n}}) \\ &= \sum_{lm}\left[\frac{(l+2)!}{(l-2)!}\right]^{1/2} E_{lm}Y_{lm}(\hat{\mathbf{n}}) \\ \tilde{B}(\hat{\mathbf{n}}) &:= \frac{i}{2}[\bar{\eth}^2(Q+iU) - \eth^2(Q-iU)] \\ &= \sum_{lm} \tilde{B}_{lm}Y_{lm}(\hat{\mathbf{n}}) \\ &= \sum_{lm}\left[\frac{(l+2)!}{(l-2)!}\right]^{1/2} B_{lm}Y_{lm}(\hat{\mathbf{n}}) \end{aligned} \tag{3.14}$$

E and B carry the same two degrees of freedom in polarisation that Q and U did, but are a lot nicer: they are defined in terms of scalars, and so are rotationally invariant and carry physical meaning.

3.1.1 Parity

We begin to uncover the physical meaning of E and B modes by showing they have opposite parity. Consider a space inversion reversing the sign of the x coordinate. In spherical coordinates this leaves r, θ invariant, but varies $\phi \to -\phi$. Let $\hat{\mathbf{n}} \equiv (\theta, \phi)$ and $\hat{\mathbf{n}}' \equiv (\theta', \phi')$ refer to the same physical direction in the two frames. From the definition of the Stokes parameters $Q = \langle|E_x|^2\rangle - \langle|E_y|^2\rangle$ and $U = \langle E_x E_y^*\rangle + \langle E_y E_x^*\rangle$ we see $Q'(\hat{\mathbf{n}}') = Q(\hat{\mathbf{n}})$ but $U'(\hat{\mathbf{n}}') = -U(\hat{\mathbf{n}})$. Thus $(Q \pm iU)'(\hat{\mathbf{n}}') = (Q \mp iU)(\hat{\mathbf{n}})$. Now by 3.14 we should act with spin raising and lowering operators twice. Acting once, using B.2

$$\begin{aligned} \bar{\eth}(Q+iU)'(\hat{\mathbf{n}}') &= -\sin^{-2}\theta'[\partial_{\theta'} - i\csc\theta'\partial_{\phi'}]\sin^2\theta'(Q+iU)'(\hat{\mathbf{n}}') \\ &= -\sin^{-2}\theta[\partial_\theta + i\csc\theta\partial_\phi]\sin^2\theta(Q-iU)'(\hat{\mathbf{n}}) \\ &= \eth(Q-iU)(\hat{\mathbf{n}}) \end{aligned} \tag{3.15}$$

applying the operator once more gives

$$\bar{\eth}^2(Q+iU)'(\hat{\mathbf{n}}') = \eth^2(Q-iU)(\hat{\mathbf{n}}) \tag{3.16}$$

and similarly

$$\eth^2(Q-iU)'(\hat{\mathbf{n}}') = \bar{\eth}^2(Q+iU)(\hat{\mathbf{n}}) \tag{3.17}$$

so we see from 3.14 that under parity $\tilde{E}'(\hat{\mathbf{n}}') = \tilde{E}(\hat{\mathbf{n}})$ but $\tilde{B}'(\hat{\mathbf{n}}') = -\tilde{B}(\hat{\mathbf{n}})$. Using the parity properties of (spin-weighted) spherical harmonics $Y_{lm} \to (-1)^l Y_{lm}$, we find multipoles transform as

$$E_{lm} \to (-1)^l E_{lm} \qquad B_{lm} \to (-1)^{l+1} B_{lm} \qquad T_{lm} \to (-1)^l T_{lm} \tag{3.18}$$

This property is the important distinguishing feature of E and B modes, and explains the nomenclature. It is in analogy with the electric and magnetic field, which transform as $E \to E$ and $B \to -B$ under parity too. We can use this property to distinguish E and B modes diagrammatically.

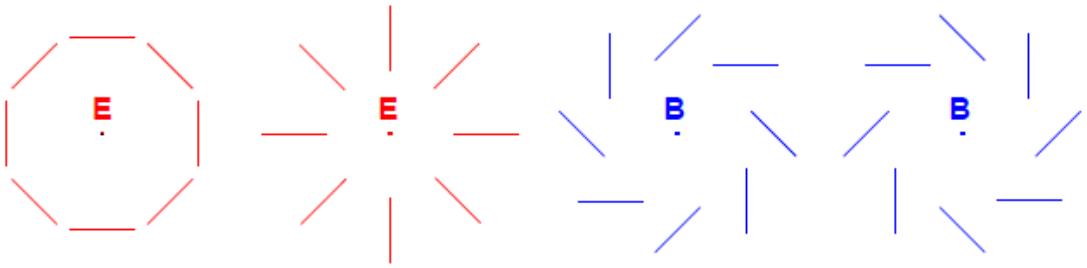

Figure 1. Typical E or B mode polarisation patterns. The electric and magnetic modes are distinguished by their behaviour under reflection.

3.1.2 Statistics

In this section we define the angular power spectra of interest. Since primordial perturbations from inflation are expected to be Gaussian, and since linear theory is a very good approximation in the early universe pre recombination, we also expect the small anisotropies in the CMB fields to be Gaussian, with zero mean.

$$\langle T_{lm} \rangle = \langle E_{lm} \rangle = \langle B_{lm} \rangle = 0 \tag{3.19}$$

These three sets of moments define the full temperature and polarisation map. By Gaussianity, all their statistical properties are contained in their angular power spectra, which by statistical isotropy take form

$$\begin{aligned}
\langle T^*_{lm} T_{l'm'} \rangle &= C_l^{TT} \delta_{ll'} \delta_{mm'} \\
\langle E^*_{lm} E_{l'm'} \rangle &= C_l^{EE} \delta_{ll'} \delta_{mm'} \\
\langle B^*_{lm} B_{l'm'} \rangle &= C_l^{BB} \delta_{ll'} \delta_{mm'} \\
\langle T^*_{lm} E_{l'm'} \rangle &= C_l^{TE} \delta_{ll'} \delta_{mm'} \\
\langle T^*_{lm} B_{l'm'} \rangle &= \langle E^*_{lm} B_{l'm'} \rangle = 0
\end{aligned} \tag{3.20}$$

The last line follows from the parity invariance of power spectra and the parity of T, E and B modes. We can write down unbiased estimators for these as

$$\hat{C}_l^{XY} = \frac{1}{2l+1} \sum_m X^*_{lm} Y_{lm} \tag{3.21}$$

for $X, Y \in \{T, E, B\}$. Their variance may be easily calculated via Wick

$$\text{var } \hat{C}_l^{XX} = \frac{2}{2l+1} C_l^{XX} C_l^{XX} \tag{3.22}$$

for $X = Y$

$$\text{var } \hat{C}_l^{XY} = \frac{1}{2l+1}(C_l^{XY}C_l^{XY} - C_l^{XX}C_l^{YY}) \tag{3.23}$$

for $X \neq Y$. In this context this sample variance is known as *cosmic variance*, and is due to the limit on the number of observable large scale, low l modes.

3.1.3 The Flat Sky Approximation

The flat sky approximation is the small scale limit of the above discussion. It neglects the curvature of the sphere, allowing us to work instead with a standard flat space Fourier basis, instead of (spin-weighted) spherical harmonics. It is a reasonable approximation on small angular scales, and also provides a useful tool to give intuition about physical effects, which we make use of when we discuss lensing in section 4.3. It is also historically relevant: much of the early work on CMB polarisation focussed on this limit, before the techniques discussed above to deal with the full sky were discovered [12].

Here, we'll describe how to get the small scale limit out of the full sky treatment. We take $\hat{\mathbf{n}}$ to be close to $\hat{\mathbf{z}}$, and make the substitutions

$$\begin{aligned} Y_{lm}(\hat{\mathbf{n}}) &\to e^{i\mathbf{l}\cdot\hat{\mathbf{n}}} \\ \sum_{lm} &\to \int \frac{d^2\mathbf{l}}{(2\pi)^2} \end{aligned} \tag{3.24}$$

leading to temperature anisotropies

$$T(\hat{\mathbf{n}}) = \sum_{lm} T_{lm}Y_{lm}(\hat{\mathbf{n}}) \to \int \frac{d^2\mathbf{l}}{(2\pi)^2} T(\mathbf{l})e^{i\mathbf{l}\cdot\hat{\mathbf{n}}} \tag{3.25}$$

and spin weighted spherical harmonics becoming, since l is large

$$\begin{aligned} {}_2Y_{lm} &= \left[\frac{(l+2)!}{(l-2)!}\right]^{\frac{1}{2}} \eth^2 Y_{lm} \to \frac{1}{l^2}\eth^2 e^{i\mathbf{l}\cdot\hat{\mathbf{n}}} \\ {}_{-2}Y_{lm} &= \left[\frac{(l+2)!}{(l-2)!}\right]^{\frac{1}{2}} \bar{\eth}^2 Y_{lm} \to \frac{1}{l^2}\bar{\eth}^2 e^{i\mathbf{l}\cdot\hat{\mathbf{n}}} \end{aligned} \tag{3.26}$$

and so polarisation becomes

$$\begin{aligned} (Q+iU)(\hat{\mathbf{n}}) &= -\int \frac{d^2\mathbf{l}}{(2\pi)^2}[E(\mathbf{l}) + iB(\mathbf{l})]\frac{1}{l^2}\eth^2 e^{i\mathbf{l}\cdot\hat{\mathbf{n}}} \\ (Q-iU)(\hat{\mathbf{n}}) &= -\int \frac{d^2\mathbf{l}}{(2\pi)^2}[E(\mathbf{l}) - iB(\mathbf{l})]\frac{1}{l^2}\bar{\eth}^2 e^{i\mathbf{l}\cdot\hat{\mathbf{n}}} \end{aligned} \tag{3.27}$$

In the small scale limit we can derive using B.2

$$\begin{aligned} \frac{1}{l^2}\eth^2 e^{i\mathbf{l}\cdot\hat{\mathbf{n}}} &= -e^{-2i(\phi-\phi_\mathbf{l})}e^{i\mathbf{l}\cdot\hat{\mathbf{n}}} \\ \frac{1}{l^2}\bar{\eth}^2 e^{i\mathbf{l}\cdot\hat{\mathbf{n}}} &= -e^{2i(\phi-\phi_\mathbf{l})}e^{i\mathbf{l}\cdot\hat{\mathbf{n}}} \end{aligned} \tag{3.28}$$

where $\phi_\mathbf{l}$ is the angle between $\mathbf{l}$ and $\hat{\mathbf{e}}_x$. So far we have been evaluating Q and U in the natural basis $(\hat{\mathbf{e}}_\theta, \hat{\mathbf{e}}_\phi)$ on the sphere. On the flat sky however we should instead consider a fixed basis $(\hat{\mathbf{e}}_x, \hat{\mathbf{e}}_y)$ orthonormal to $\hat{\mathbf{z}}$. We may rotate between them using 3.6: $Q' \pm iU' = e^{\mp 2i\phi}(Q \pm iU)$, finding after dropping the prime

$$\begin{aligned} Q(\hat{\mathbf{n}}) &= \int \frac{d^2\mathbf{l}}{(2\pi)^2}[E(\mathbf{l})\cos 2\phi_\mathbf{l} - B(\mathbf{l})\sin 2\phi_\mathbf{l}]e^{i\mathbf{l}\cdot\hat{\mathbf{n}}} \\ U(\hat{\mathbf{n}}) &= \int \frac{d^2\mathbf{l}}{(2\pi)^2}[E(\mathbf{l})\sin 2\phi_\mathbf{l} + B(\mathbf{l})\cos 2\phi_\mathbf{l}]e^{i\mathbf{l}\cdot\hat{\mathbf{n}}} \end{aligned} \tag{3.29}$$

i.e. E and B modes are related to Q and U modes by a rotation in Fourier space, as defined in [8]

$$\begin{pmatrix} Q(\mathbf{l}) \\ U(\mathbf{l}) \end{pmatrix} = \begin{pmatrix} \cos 2\phi_{\mathbf{l}} & -\sin 2\phi_{\mathbf{l}} \\ \sin 2\phi_{\mathbf{l}} & \cos 2\phi_{\mathbf{l}} \end{pmatrix} \begin{pmatrix} E(\mathbf{l}) \\ B(\mathbf{l}) \end{pmatrix} \tag{3.30}$$

More compactly

$$(Q \pm iU)(\mathbf{l}) = e^{\pm 2i\phi_{\mathbf{l}}}(E \pm iB)(\mathbf{l}) \tag{3.31}$$

From this we can get a better intuitive understanding of what E and B modes are. We see for a pure B mode in the $\hat{\mathbf{x}}$ direction where $\phi_{\mathbf{l}} = 0$ that $Q(\mathbf{l}) = 0$ while $U(\mathbf{l}) = B(\mathbf{l})$. For a pure E mode on the other hand, we get $Q(\mathbf{l}) = E(\mathbf{l})$ and $U(\mathbf{l}) = 0$. So for an E mode, the polarization varies parallel/perpendicular to the direction of the Fourier mode, while for a B mode it varies along directions at 45°to the Fourier mode, as shown in figure 2 with headless vectors.

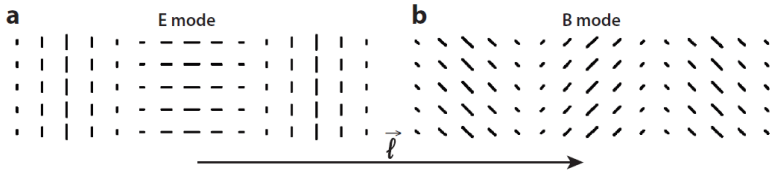

Figure 2. Polarization patterns associated with (a) a single E mode and (b) a single B mode with horizontal wavevector $\mathbf{l}$. By C. Bischoff and taken from [13].

3.2 Inflationary Gravitational Waves

Having discussed the relevant polarisation observables, we now wish to understand how they relate to our primordial inflationary spectra. The main goal of this section is to show that tensor perturbations source a non zero B mode polarisation, whose power spectrum depends on the primordial tensor power spectrum. We present the argument laid out in [12], though see also [10] which rigorously derives the Boltzmann equations.

It is most convenient throughout to work in Fourier space with wave-vector $\mathbf{k}$, and to rotate our coordinate system such that this is aligned with the $\hat{\mathbf{z}}$ direction. There exist two independent polarisations of the tensor perturbation for our Fourier mode: ξ^+ and $\xi^\times$. We may choose simple polarisation vectors $e^+_{xx} = -e^+_{yy} = 1$ and $e^\times_{xy} = e^\times_{yx} = 1$ with all other components 0. In a cosmological context we take these modes to have equal amplitude i.e. $\xi^+(\mathbf{k}, \tau) = \xi^\times(\mathbf{k}, \tau) = h(\mathbf{k}, \tau)$ and it is convenient to repackage them as

$$\xi^1 = (\xi^+ - i\xi^\times)/\sqrt{2} \qquad \xi^2 = (\xi^+ + i\xi^\times)/\sqrt{2} \tag{3.32}$$

At $\tau = 0$, inflation tells us our initial frozen modes ξ^+ and $\xi^\times$ are independent, and drawn from a Gaussian variate, whose individual power spectra are half of the total tensor power spectrum 2.21. Our new variables, being linearly independent combinations of ξ^s, are also Gaussian, and a short calculation reveals they are also independent, each with half of the the total primordial tensor power, i.e. at $\tau = 0$

$$\begin{gathered} \langle \xi^{1*}(\mathbf{k})\xi^1(\mathbf{k}')\rangle = \langle \xi^{2*}(\mathbf{k})\xi^2(\mathbf{k}')\rangle = (2\pi)^3\delta(\mathbf{k}-\mathbf{k}')\frac{P_t(k)}{2} \\ \langle \xi^{1*}(\mathbf{k})\xi^2(\mathbf{k}')\rangle = 0 \end{gathered} \tag{3.33}$$

where $P_t(k) = \frac{2\pi^2}{k^3}\Delta^2_t(k)$ is the standard dimensionfull power spectrum. Note our fourier convention differs from [12], which will give us a different final angular power spectrum.

To completely understand the full photon distribution we must follow the evolution of four distributions f_X, one for each Stokes parameter $X \in \{I, Q, U, V\}$. Thomson scattering of anisotropic radiation

by free electrons gives rise to only linear polarization, so we may safely ignore f_V. This can be seen mathematically by verifying the V Boltzmann equation has no source term [10]. For homogeneous and isotropic unpolarised radiation the distribution is simply $\bar{f}_I(\tau) = [e^{\hbar\nu/k_b T(\tau)} - 1]^{-1}$, $f_Q = f_U = 0$, the black body Planck distribution. The presence of metric perturbations breaks this homogeneity, inducing at linear order frequency independent perturbations $\Delta_X(\tau, \hat{\mathbf{n}}, \mathbf{x})$ in real space or $\Delta_X(\tau, \hat{\mathbf{n}}, \mathbf{k})$ in Fourier space. Here, $\hat{\mathbf{n}}$ is the line of sight, $\mathbf{x}$ denotes spatial position, with conjugate $\mathbf{k}$, and τ is conformal time. In principle these anisotropies additionally have frequency dependence, but since spectral distortions are second order we may ignore them at linear order. Let θ and ϕ be spherical angles around $\hat{\mathbf{z}}$ (or equivalently $\mathbf{k}$) parameterising $\hat{\mathbf{n}}$, and measure Q and U in their natural basis $(\hat{\mathbf{e}}_\theta, \hat{\mathbf{e}}_\phi)$ on the sphere. The intensity anisotropy may be related to the temperature anisotropy via $\Delta_I/4 = \Delta_T = \frac{\delta T}{\bar{T}}$. Following a method first introduced by Polnarev [14], we introduce new variables $\tilde{\Delta}_T(\tau, \mu, k)$ and $\tilde{\Delta}_P(\tau, \mu, k)$ with simpler angular dependence to describe temperature and polarisation anisotropies, depending only on $\mu = \hat{\mathbf{n}} \cdot \hat{\mathbf{k}} = \cos\theta$ rather than on both θ and ϕ. They are related to our original variables via

$$\begin{aligned}
\Delta_T(\tau, \hat{\mathbf{n}}, \mathbf{k}) &= [(1-\mu^2)e^{2i\phi}\xi^1(\mathbf{k}) + (1-\mu^2)e^{-2i\phi}\xi^2(\mathbf{k})]\tilde{\Delta}_T(\tau, \mu, k) \\
(\Delta_Q + i\Delta_U)(\tau, \hat{\mathbf{n}}, \mathbf{k}) &= [(1-\mu)^2 e^{2i\phi}\xi^1(\mathbf{k}) + (1+\mu)^2 e^{-2i\phi}\xi^2(\mathbf{k})]\tilde{\Delta}_P(\tau, \mu, k) \\
(\Delta_Q - i\Delta_U)(\tau, \hat{\mathbf{n}}, \mathbf{k}) &= [(1+\mu)^2 e^{2i\phi}\xi^1(\mathbf{k}) + (1-\mu)^2 e^{-2i\phi}\xi^2(\mathbf{k})]\tilde{\Delta}_P(\tau, \mu, k)
\end{aligned} \tag{3.34}$$

and obey at linear order *decoupled* Boltzmann equations given by [14]

$$\begin{aligned}
\tilde{\Delta}_T' + ik\mu\tilde{\Delta}_T &= -h' - \kappa'[\tilde{\Delta}_T - \Psi] \\
\tilde{\Delta}_P' + ik\mu\tilde{\Delta}_P &= -\kappa'[\tilde{\Delta}_P + \Psi]
\end{aligned} \tag{3.35}$$

where the source is

$$\Psi = \frac{1}{10}\tilde{\Delta}_{T0} + \frac{1}{7}\tilde{\Delta}_{T2} + \frac{3}{70}\tilde{\Delta}_{T4} - \frac{3}{5}\tilde{\Delta}_{P0} + \frac{6}{7}\tilde{\Delta}_{P2} - \frac{3}{70}\tilde{\Delta}_{P4} \tag{3.36}$$

written in terms of moments, given by $\Delta(k, \mu) = \sum_l (2l+1)(-i)^l \Delta_l(k) P_l(\mu)$ for $P_l(\mu)$ the order l Legendre polynomial. All derivatives are taken with respect to conformal time τ. h is the gravitational wave amplitude. κ is the Thomson optical depth, described in more detail in the next section. These equations encode relatively simple physics. The left hand sides are simply the Lagrangian time derivatives of a Fourier mode with wave number k. The h' in the first equation encodes the temperature variation induced by the gravitational wave. While not present explicitly in the polarisation equation, it also affects it through the source term Ψ, which depends on moments of the temperature fluctuation. The terms multiplying κ' come from the Thomson scattering collision term of the Boltzmann equation, and are derived using the angular dependence of the Thomson differential cross section from QED [10, 13].

By multiplying the Boltzmann equations 3.35 by $P_l(\mu)$ and integrating over angular dependence μ, making use of the relevant identities for Legendre polynomials, we obtain a heirachy of equations connecting higher moments to lower, a fact we will use later.

3.2.1 Optical Depth

While the Universe is young and hot, baryons are ionised and tightly coupled to photons via Thomson scattering. Once the temperature falls below a few eV, it becomes favourable for electrons and ions to 'recombine' into neutral molecules. As the number of charged particles falls, the mean free path photons increases. Eventually, the mean free path becomes comparable to the horizon size and the photon and baryon fluids decouple. It is at this point in the Universe's evolution that the CMB photons last scatter [15].

To describe this mathematically, we define the differential optical depth and optical depth

$$\kappa' = a n_e x_e \sigma_T \qquad \kappa(\tau) = \int_\tau^{\tau_0} \kappa'(\tau') d\tau' \tag{3.37}$$

where a is the scale factor, n_e the electron number density, x_e the ionization fraction, and σ_T the Thomson cross section. Note here $\kappa' = -\frac{d\kappa}{d\tau}$ differs from the conformal time derivative by a minus sign to match the conventions of [12, 16] - this is the only quantity for which this convention is used. We have limiting values $\kappa(\tau_0) = 0$ and $\kappa(0) \to \infty$ today and in the far past.

The visibility function describes the probability density that a given CMB photon last scattered at a particular time τ. It is given terms of the above quantities as

$$g(\tau) = \kappa' e^{-\kappa} \tag{3.38}$$

Numerical calculations show that $g(\tau)$ is sharply peaked around recombination. Noting by definition, g must integrate to unity, the simplest approximation takes it to be a delta function, and bears the name 'instantaneous recombination', as every photon decouples at the same time. The next simplest approximation is to take the visibility function to be a narrow Gaussian

$$g(\tau) = g(\tau_R) e^{-\frac{(\tau-\tau_R)^2}{2\Delta\tau_R^2}} \tag{3.39}$$

where τ_R is the time of recombination, $\Delta\tau_R$ is its width, and $g(\tau_R)$ is the amplitude. We will also make use of an approximation for the optical depth during recombination. Writing $\kappa = e^{-f(\tau)}$, consistency between 3.38 and 3.39 requires $\kappa \approx e^{-(\tau-\tau_R)/\Delta\tau_R}$ and $g(\tau_R) \approx 1/(e\Delta\tau_R)$ near τ_R.

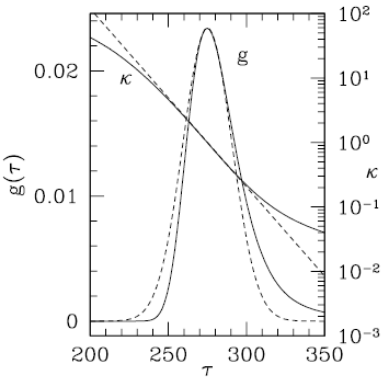

Figure 3. Recombination history. Plotted are the visibility function and optical depth calculated numerically in bold, and the Gaussian approximation with $\Delta\tau_R = 15.7$, dashed. Figure from [15].

This is a decent approximation for the visibility function but we find it isn't quite right. In particular, after the 'dark ages' in which the universe is very neutral, we know from observations of quasar absorption spectra that the universe is highly ionized again at $5 < z < 20$. This reionization is driven by radiation from the first stars interacting with hot hydrogen gas. CMB photons therefore enter a second phase of Thomson scattering at a later time [17], which is important to account for in our CMB theory.

3.2.2 Line of Sight Expressions

While one may solve the Boltzmann heirachy directly from initial conditions, it proves more instructive, intuitive and numerically effiecent to use the 'line of sight method', first introduced in [16], to predict measured values of the CMB fields on earth today. We formally integrate these first order linear ODEs along the photon path, making use of an integrating factor $e^{\int d\tau(ik\mu+\kappa')} = e^{ik\mu\tau-\kappa}$ (by $\kappa' = -\frac{d\kappa}{d\tau}$), from their initial conditions to now. Introducing $x = k(\tau_0 - \tau)$ we get

$$\begin{aligned}\tilde{\Delta}_T(\tau_0, \mu, k) &= \int_0^{\tau_0} d\tau e^{-ix\mu} S_T(k, \tau) \\ \tilde{\Delta}_P(\tau_0, \mu, k) &= \int_0^{\tau_0} d\tau e^{-ix\mu} S_P(k, \tau)\end{aligned} \tag{3.40}$$

after multiplying by the integrating factor, integrating, making use of $\kappa(\tau_0) = 0$ and $\kappa(0) \to \infty$ to evaluate the left hand side limits, and finally dividing through by $e^{ik\mu\tau_0}$. All the physics is hidden in the source terms

$$\begin{aligned} S_T(k,\tau) &= -h' e^{-\kappa} + g\Psi \\ S_P(k,\tau) &= -g\Psi \end{aligned} \tag{3.41}$$

which we'll explore in section 3.3. This let's us write

$$\begin{aligned} \Delta_T(\tau_0, \hat{\mathbf{n}}, \mathbf{k}) &= [(1-\mu^2)e^{2i\phi}\xi^1(\mathbf{k}) + (1-\mu^2)e^{-2i\phi}\xi^2(\mathbf{k})] \int_0^{\tau_0} d\tau e^{-ix\mu} S_T(k,\tau) \\ (\Delta_Q + i\Delta_U)(\tau_0, \hat{\mathbf{n}}, \mathbf{k}) &= [(1-\mu)^2 e^{2i\phi}\xi^1(\mathbf{k}) + (1+\mu)^2 e^{-2i\phi}\xi^2(\mathbf{k})] \int_0^{\tau_0} d\tau e^{-ix\mu} S_P(k,\tau) \\ (\Delta_Q - i\Delta_U)(\tau_0, \hat{\mathbf{n}}, \mathbf{k}) &= [(1+\mu)^2 e^{2i\phi}\xi^1(\mathbf{k}) + (1-\mu)^2 e^{-2i\phi}\xi^2(\mathbf{k})] \int_0^{\tau_0} d\tau e^{-ix\mu} S_P(k,\tau) \end{aligned} \tag{3.42}$$

The T result is what we want. Recall Q and U however are coordinate dependent quantities on the sphere. We work instead with $\tilde{E}$ and $\tilde{B}$. 3.14 tells us to convert between them all we need to do is act twice via our raising and lowering operators. Making of B.3, which conveniently pass through the source terms with no angular dependence, we get

$$\begin{aligned} \bar{\eth}^2(\Delta_Q + i\Delta_U)(\tau_0, \hat{\mathbf{n}}, \mathbf{k}) &= +\xi^1(\mathbf{k})e^{2i\phi} \int_0^{\tau_0} d\tau S_P(k,\tau)(-\partial_\mu + \frac{2}{1-\mu^2})^2[(1-\mu^2)(1-\mu)^2 e^{-ix\mu}] \\ &\quad + \xi^2(\mathbf{k})e^{-2i\phi} \int_0^{\tau_0} d\tau S_P(k,\tau)(-\partial_\mu - \frac{2}{1-\mu^2})^2[(1-\mu^2)(1+\mu)^2 e^{-ix\mu}] \\ &= -\xi^1(\mathbf{k})e^{2i\phi} \int_0^{\tau_0} d\tau S_P(k,\tau)(\hat{\mathcal{E}}(x) - i\hat{\mathcal{B}}(x))[(1-\mu^2)e^{-ix\mu}] \\ &\quad - \xi^2(\mathbf{k})e^{-2i\phi} \int_0^{\tau_0} d\tau S_P(k,\tau)(\hat{\mathcal{E}}(x) + i\hat{\mathcal{B}}(x))[(1-\mu^2)e^{-ix\mu}] \end{aligned} \tag{3.43}$$

$$\begin{aligned} \eth^2(\Delta_Q - i\Delta_U)(\tau_0, \hat{\mathbf{n}}, \mathbf{k}) &= +\xi^1(\mathbf{k})e^{2i\phi} \int_0^{\tau_0} d\tau S_P(k,\tau)(-\partial_\mu - \frac{2}{1-\mu^2})^2[(1-\mu^2)(1+\mu)^2 e^{-ix\mu}] \\ &\quad + \xi^2(\mathbf{k})e^{-2i\phi} \int_0^{\tau_0} d\tau S_P(k,\tau)(-\partial_\mu + \frac{2}{1-\mu^2})^2[(1-\mu^2)(1-\mu)^2 e^{-ix\mu}] \\ &= -\xi^1(\mathbf{k})e^{2i\phi} \int_0^{\tau_0} d\tau S_P(k,\tau)(\hat{\mathcal{E}}(x) + i\hat{\mathcal{B}}(x))[(1-\mu^2)e^{-ix\mu}] \\ &\quad - \xi^2(\mathbf{k})e^{-2i\phi} \int_0^{\tau_0} d\tau S_P(k,\tau)(\hat{\mathcal{E}}(x) - i\hat{\mathcal{B}}(x))[(1-\mu^2)e^{-ix\mu}] \end{aligned} \tag{3.44}$$

where we have introduced differential operators, which will save us some work very soon.

$$\hat{\mathcal{E}}(x) = -12 + x^2(1-\partial_x^2) - 8x\partial_x \qquad \hat{\mathcal{B}}(x) = 8x + 2x^2\partial_x \tag{3.45}$$

Plugging these into 3.14 we find our final results for each Fourier mode to be

$$\begin{aligned} \Delta_T(\tau_0, \hat{\mathbf{n}}, \mathbf{k}) &= [(1-\mu^2)e^{2i\phi}\xi^1(\mathbf{k}) + (1-\mu^2)e^{-2i\phi}\xi^2(\mathbf{k})] \int_0^{\tau_0} d\tau e^{-ix\mu} S_T(k,\tau) \\ \Delta_{\tilde{E}}(\tau_0, \hat{\mathbf{n}}, \mathbf{k}) &= [(1-\mu^2)e^{2i\phi}\xi^1(\mathbf{k}) + (1-\mu^2)e^{-2i\phi}\xi^2(\mathbf{k})]\hat{\mathcal{E}}(x) \int_0^{\tau_0} d\tau e^{-ix\mu} S_P(k,\tau) \\ \Delta_{\tilde{B}}(\tau_0, \hat{\mathbf{n}}, \mathbf{k}) &= [(1-\mu^2)e^{2i\phi}\xi^1(\mathbf{k}) + (1-\mu^2)e^{-2i\phi}\xi^2(\mathbf{k})]\hat{\mathcal{B}}(x) \int_0^{\tau_0} d\tau e^{-ix\mu} S_P(k,\tau) \end{aligned} \tag{3.46}$$

The complete solution requires integration over all Fourier modes, which evolve independently. Note the phase factor vanishes as we evaluate all terms at the same spatial position $\mathbf{x} = 0$

$$\begin{aligned}\Delta_T(\tau_0, \hat{\mathbf{n}}) &= \int \frac{d^3\mathbf{k}}{(2\pi)^3}\Delta_T(\tau_0, \hat{\mathbf{n}}, \mathbf{k}) \\ \Delta_{\tilde{E}}(\tau_0, \hat{\mathbf{n}}) &= \int \frac{d^3\mathbf{k}}{(2\pi)^3}\Delta_{\tilde{E}}(\tau_0, \hat{\mathbf{n}}, \mathbf{k}) \\ \Delta_{\tilde{B}}(\tau_0, \hat{\mathbf{n}}) &= \int \frac{d^3\mathbf{k}}{(2\pi)^3}\Delta_{\tilde{B}}(\tau_0, \hat{\mathbf{n}}, \mathbf{k})\end{aligned} \tag{3.47}$$

If we had chosen to work with Q and U here, in order to sum up Fourier modes with respect to a fixed basis with respect to the sphere, we would need to rotate each $Q \pm iU$ $\mathbf{k}$ mode by a $\mathbf{k}$ and $\hat{\mathbf{n}}$ dependent phase (since we aligned $\mathbf{k}$ with $\hat{\mathbf{z}}$). This was a complication in early attempts to characterise the CMB polarisation beyond the flat sky regime, and we have avoided it through our definition of rotationally invariant E and B modes.

3.2.3 Tensor Power Spectra

We see tensor perturbations have induced both E and B modes. Thankfully the form of these expressions are very similar, allowing us to compute all the power spectra in one go. We'll begin by calculating the TT power spectrum C_l^{TT} sourced by tensor perturbations. Using the expression for spherical multipole coefficients

$$T_{lm} = \int d\Omega Y^*_{lm}(\hat{\mathbf{n}})\Delta_T(\tau_0, \hat{\mathbf{n}}) \tag{3.48}$$

and making use of 3.20 we can write

$$\begin{aligned}C_l^{TT} &= \frac{1}{2l+1}\sum_m \langle T^*_{lm}T_{lm}\rangle \\ &\supset \frac{4\pi}{2l+1}\int \frac{k^2dk}{(2\pi)^3}\frac{P_t(k)}{2}\sum_m \left|\int d\Omega Y^*_{lm}(\hat{\mathbf{n}})\int_0^{\tau_0} d\tau S_T(k,\tau)(1-\mu^2)e^{2i\phi}e^{-ix\mu}\right|^2 \\ &= 2\pi^2\left[\frac{(l-2)!}{(l+2)!}\right]\int \frac{k^2dk}{(2\pi)^3}P_t(k)\left|\int_0^{\tau_0} d\tau S_T(k,\tau)\int_{-1}^{1} d\mu P_l^2(\mu)(1-\mu^2)e^{-ix\mu}\right|^2 \\ &= 2\pi^2\left[\frac{(l-2)!}{(l+2)!}\right]\int \frac{k^2dk}{(2\pi)^3}P_t(k)\left|\int_0^{\tau_0} d\tau S_T(k,\tau)\int_{-1}^{1} d\mu \partial_\mu^2 P_l(\mu)(1-\mu^2)^2e^{-ix\mu}\right|^2 \\ &= 2\pi^2\left[\frac{(l-2)!}{(l+2)!}\right]\int \frac{k^2dk}{(2\pi)^3}P_t(k)\left|\int_0^{\tau_0} d\tau S_T(k,\tau)\int_{-1}^{1} d\mu \partial_\mu^2 P_l(\mu)(1+\partial_x^2)^2e^{-ix\mu}\right|^2 \\ &= 2\pi^2\left[\frac{(l-2)!}{(l+2)!}\right]\int \frac{k^2dk}{(2\pi)^3}P_t(k)\left|\int_0^{\tau_0} d\tau S_T(k,\tau)\int_{-1}^{1} d\mu P_l(\mu)(1+\partial_x^2)^2(x^2e^{-ix\mu})\right|^2 \\ &= 2\pi^2\left[\frac{(l-2)!}{(l+2)!}\right]\int \frac{k^2dk}{(2\pi)^3}P_t(k)\left|\int_0^{\tau_0} d\tau S_T(k,\tau)(1+\partial_x^2)^2\left(x^2\int_{-1}^{1} d\mu P_l(\mu)e^{-ix\mu}\right)\right|^2 \\ &= 8\pi^2\left[\frac{(l-2)!}{(l+2)!}\right]\int \frac{k^2dk}{(2\pi)^3}P_t(k)\left|\int_0^{\tau_0} d\tau S_T(k,\tau)(1+\partial_x^2)^2\left(x^2 j_l(x)\right)\right|^2 \\ &= 8\pi^2\left[\frac{(l+2)!}{(l-2)!}\right]\int \frac{k^2dk}{(2\pi)^3}P_t(k)\left|\int_0^{\tau_0} d\tau S_T(k,\tau)\frac{j_l(x)}{x^2}\right|^2\end{aligned} \tag{3.49}$$

Where we have used the statistical properties 3.33 of $\xi^i(\mathbf{k})$ to compute the primordial expectation value. For readability we have only included the piece arising from ξ^1. The piece arising from ξ^2 differs in the second line by replacing $e^{2i\phi}$ with its complex conjugate $e^{-2i\phi}$, and can easily be shown to contribute exactly the same, using properties of P_l^m (omitted). The power spectra is therefore

twice the result above.

To evaluate the angular integrals, we used the expression for spherical harmonics in terms of associated legendre polynomials.

$$Y_{lm} = \left[\frac{(2l+1)(l-m)!}{4\pi(l+m)!}\right]^{\frac{1}{2}} P_l^m(\mu)e^{-im\phi} \tag{3.50}$$

The ϕ integral vanishes unless $m = 2$, in which case it gives 2π. Then, for the μ integral we make use of

$$P_l^m(\mu) = (-1)^m(1-\mu^2)^{m/2}(\partial_\mu)^m P_l(\mu) \tag{3.51}$$

and integrate by parts twice giving the factor of x^2. Then we use

$$\int_{-1}^{1} d\mu e^{-ix\mu} P_l(\mu) = 2(-i)^l j_l(x) \tag{3.52}$$

to perform the μ integral. Finally we make use of the differential equation

$$j_l'' + \frac{2j_l'}{x} + \left(1 - \frac{l(l+1)}{x^2}\right) j_l = 0 \tag{3.53}$$

to eliminate derivatives of bessel functions and obtain

$$(1+\partial_x^2)^2[x^2 j_l(x)] = (l-1)l(l+1)(l+1)\frac{j_l}{x^2} \tag{3.54}$$

explaining the change in the l dependent prefactor in the last line.

This gives final result for the temperature power spectrum. Now we abuse the similarity of expressions in 3.46 to write down the EE and BB power spectra. The angular dependence of $\Delta_{\tilde{E}}$ and $\Delta_{\tilde{B}}$ are exactly the same as those of Δ_T, with the expressions only differing in the operators $\hat{\mathcal{E}}$ and $\hat{\mathcal{B}}$, acting seperately on each $\mathbf{k}$ mode, which can be applied after the angular integrals are performed. We lose the l dependent factor in front by converting from $\tilde{E}, \tilde{B}$ to E, B, using 3.14

$$\begin{aligned}
C_l^{EE} &= (4\pi)^2 \int \frac{k^2 dk}{(2\pi)^3} P_t(k) \left| \int_0^{\tau_0} d\tau S_P(k,\tau)\hat{\mathcal{E}}(x)\frac{j_l(x)}{x^2}\right|^2 \\
&= (4\pi)^2 \int \frac{k^2 dk}{(2\pi)^3} P_t(k) \left| \int_0^{\tau_0} d\tau S_P(k,\tau)[-j_l(x) + j_l''(x) + \frac{2j_l(x)}{x^2} + \frac{4j_l'(x)}{x}]\right|^2 \\
C_l^{BB} &= (4\pi)^2 \int \frac{k^2 dk}{(2\pi)^3} P_t(k) \left| \int_0^{\tau_0} d\tau S_P(k,\tau)\hat{\mathcal{B}}(x)\frac{j_l(x)}{x^2}\right|^2 \\
&= (4\pi)^2 \int \frac{k^2 dk}{(2\pi)^3} P_t(k) \left| \int_0^{\tau_0} d\tau S_P(k,\tau)[2j_l'(x) + \frac{4j_l(x)}{x}]\right|^2
\end{aligned} \tag{3.55}$$

Having computed these, we may repackage these power spectra neatly by reading off the multipole moments due to a single wave number k as

$$\begin{aligned}
\Delta_{Tl}(k) &= \left[\frac{(l+2)!}{(l-2)!}\right]^{\frac{1}{2}} \int_0^{\tau_0} d\tau \left(-h'(\tau)e^{-\kappa(\tau)} - g(\tau)\Psi(k,\tau)\right)\frac{j_l(x)}{x^2} \\
\Delta_{El}(k) &= \int_0^{\tau_0} d\tau \left(-g(\tau)\Psi(k,\tau)\right)\left[-j_l(x) + j_l''(x) + \frac{2j_l(x)}{x^2} + \frac{4j_l'(x)}{x}\right] \\
\Delta_{Bl}(k) &= \int_0^{\tau_0} d\tau \left(-g(\tau)\Psi(k,\tau)\right)\left[2j_l'(x) + \frac{4j_l(x)}{x}\right]
\end{aligned} \tag{3.56}$$

with $x = k(\tau_0 - \tau)$. These may be further integrated by parts to improve computational efficiency by moving derivatives off the bessel functions. Power spectra may be written in terms of these as

$$\begin{aligned} C_l^{XY} &= (4\pi)^2 \int \frac{k^2 dk}{(2\pi)^3} P_t(k) \Delta_{Xl}(k) \Delta_{Yl}(k) \\ &= 4\pi \int d\ln k \Delta_t^2(k) \Delta_{Xl}(k) \Delta_{Yl}(k) \end{aligned} \tag{3.57}$$

which are non vanishing only for $XY \in \{TE, TT, EE, BB\}$. We kept the factor of $(2\pi)^3$ explicit throughout, so that it may easily be removed to compare to [12].

3.3 Interpretation of B Mode Power Spectra

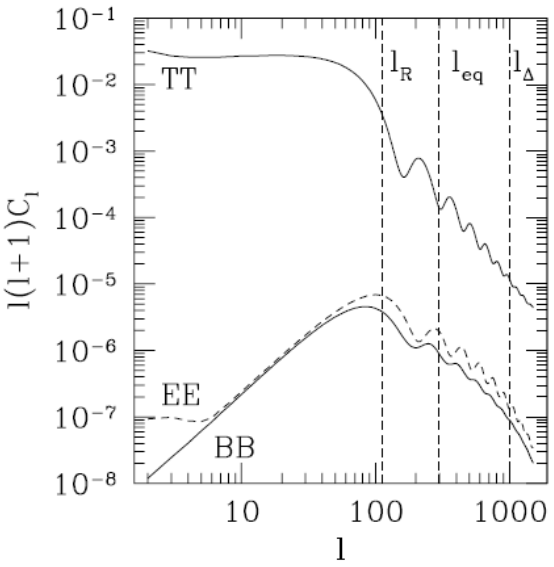

Figure 4. Tensor power spectra in reionisationless model, with vertical lines indicating the three important angular scales, horizon size at recombination τ_R, horizon size at matter-radiation equality τ_{eq} and width of last-scattering surface $\Delta\tau_R$.

Having written down expressions for the power spectra contributions of tensor modes we now wish to understand what they look like. As seen when studying CMB anisotropies, it is possible to get a good qualitative understanding for the shape of power spectra working analytically, though when percent level precision is needed a suitable numerical code must be used. This sections discussion and figures are in large part from [15], though also see [18].

To do so, we need to understand the objects in the main results above. We have already discussed the visibility function g, and will use throughout the Gaussian approximation for recombination, bearing in mind this isnt quite right and we should expect a contribution from reionisation too, discussed briefly at the end of the section. All power spectra also depend on the unknown tensor power spectrum, which control their overall amplitude, and also affect their scale dependence. For figures, we take $A_t = \frac{(2\pi)^3}{8(4\pi)^2}, n_t = 0$, and remaining cosmological parameters to be a ΛCDM cosmology with $\Omega_b = 0.05, \Omega_{DM} = 0.25, \Omega_\Lambda = 0.7$ and Hubble parameter $h = 0.72$. It remains to discuss the gravitational wave amplitude evolution h', the projection functions, and finally the source term Ψ, a function of polarisation and temperature anisotropy moments. First however we give some intuition about the expected shape of power spectra, shown in figure 4.

Temperature anisotropies

$$\Delta_{Tl} = \left[\frac{(l+2)!}{(l-2)!}\right]^{\frac{1}{2}} \int_0^{\tau_0} d\tau(-h'e^{-\kappa} + g\Psi)\frac{j_l(x)}{x^2} \tag{3.58}$$

have two contributions. The second source term is localised at the surface of last scattering (SLS) by the visibility function, and will be discussed in some detail below. It turns out to be subleading at all scales. The first is a form of integrated Sachs-Wolfe term, describing the anisotropy generated by the photon travelling through a changing gravitational potential on its path to us. Between the SLS and today, the average amplitude of the gravitational wave decreases (as it is redshifted), and so the mean energy of photon increases. Today, the gravitational wave background is negligible, and as a result, the final energy of photon is determined by whether its journey from the SLS started in a trough or crest of the tensor mode. Akin to the usual ISW effect, this term is responsible for the large scale flat nature of the TT power spectrum.

Polarisation anisotropies can be written

$$\Delta_{Xl} = \int_0^{\tau_0} d\tau(-g\Psi)P_{Xl}(k(\tau_0 - \tau)) \tag{3.59}$$

involving a single SLS localised source, and an l dependent projection function. This is sensible, as free streaming photons, while experiencing energy shifts due to cosmic expansion, should not be repolarised after last scattering. Consider photons scattering off an electron in its rest frame - the photons arrive from all directions from a mean distance determined by the mean free path at recombination. During propagation, they experience the ISW effect, discussed above, and so arrive with different temperatures, i.e. we have a temperature quadrupole which after scattering gives rise to linear polarisation.

The power spectrum can be understood as follows. By causality, the gravitational wave amplitude is constant on super horizon scales, but, like radiation, we expect it to decay rapidly upon entering the horizon. So, photons incident on modes that are super horizon at last scattering don't experience much ISW temperature change and generate little polarisation. Optimal ISW and thus maximal polarisation is generated by modes entering the horizon at the time of penultimate scattering, as this is the period in which the gravitational wave loses most of its amplitude. Translating into the form of the polarisation power spectrum, we expect to see a slow increase in power at large scales, peaking at the horizon scale at penultimate scattering. For smaller scales we expect a drop corresponding to the transition between modes entering in the penultimate to last scattering period and those not. The matter-radiation equality scale should be distinctive due to the gravitational wave amplitude exhibiting differing scaling in the two eras. On very small scales, phase cancellation, defined later but resulting in a similar effect to diffusion damping, becomes important and leads to an exponential suppression.

3.3.1 Gravitational Wave Evolution

Gravitational waves frozen after inflation become dynamical upon horizon reentry, with amplitude sourcing temperature fluctuations in the CMB. Their evolution is determined by the Einstein equation, given by [15]

$$h''_{ij} + 2\mathcal{H}h'_{ij} - \nabla^2 h_{ij} = 16\pi G a^2 \Pi_{ij} \tag{3.60}$$

where Π_{ij} is the anisotropic stress, sourced in small amounts by neutrino free-streaming. In the absence of anisotropic stress, and decomposing the tensor perturbation into its polarisation states in Fourier space we find each of h_+ and $h_\times$ satisfy

$$h'' + 2\mathcal{H}h' + k^2 h = 0 \tag{3.61}$$

which one can equivalently obtain by recalling each mode of the tensor perturbation $ah_{\mathbf{k}}$ obeys the Muhkanov-Sasaki equation A.8. Of particular interest is the matter dominated era where $\mathcal{H} = 2/\tau$. Upon performing the change of variable $x = k\tau, h = f(x)/x$ we obtain

$$x^2 \frac{d^2 f}{dx^2} + 2x \frac{df}{dx} + (x^2 - 2) f = 0 \tag{3.62}$$

which we recognise as the $l = 1$ spherical bessel equation, with regular solution $f(x) = j_1(x)$. We therefore have

$$h_{\mathbf{k}}^{\mathrm{mat}}(\tau) = 3h_{\mathbf{k}}(0) \frac{j_1(k\tau)}{k\tau} \tag{3.63}$$

The relevant quantity is the conformal time derivative of this, which we may obtain using the property

$$j_{n+1}(x) = -(-x)^n \frac{d}{dx}(-x)^{-n} j_n(x) \tag{3.64}$$

leading to

$$h_{\mathbf{k}}^{'\mathrm{mat}}(\tau) = -3h_{\mathbf{k}}(0) \frac{j_2(k\tau)}{\tau} \tag{3.65}$$

A similar method can be applied to the radiation dominated epoch, with $\mathcal{H} = 1/\tau$, to obtain

$$h_{\mathbf{k}}^{\mathrm{rad}}(\tau) = h_{\mathbf{k}}(0) j_0(k\tau) \tag{3.66}$$

The behaviour of these solutions splits into three regimes. When $k\tau \ll 1$, h evolves slowly and is approximately constant, corresponding to a frozen superhorizon mode. For $k\tau \approx 1$, the amplitude decays rapidly and settles into an oscillatory phase with decaying amplitude for $k\tau \gg 1$, corresponding to the mode enetering the horizon and redshifting away. See figure 5. Since recombination occurs shortly after matter domination, we expect the form h^{mat} to be a good description for modes entering the horizon during matter domination, though for modes entering during radiation domination we expect the radiation to matter domination transition to affect evolution significantly.

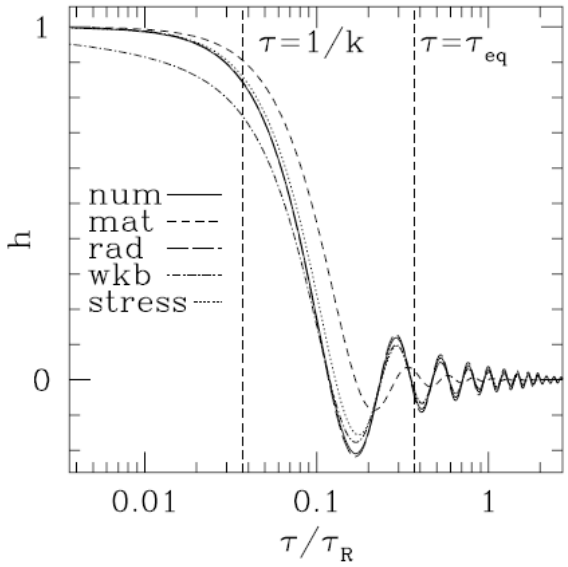

Figure 5. Gravitational wave evolution at wavenumber satisfying $k\tau_{eq} = 10$. Shown solutions are numerical without anisotropic stress, analytic matter domination, analytic radiation domination, a WKB approximation, and numerical with anisotropic stress.

Even without a complete analytical solution, we may obtain the scaling of h via a simple argument. Before horizon entry, by causality the amplitude h should be constant. After horizon entry, the gravitational wave redshifts with expansion as radiation (the graviton is massless), and scales as $h \sim 1/a$. Hence we have the relation between the gravitational wave amplitude today and at horizon entry $h_{\rm today}/h_{\rm entry} = a_{\rm today}/a_{\rm entry}$. Taking $h_{\rm entry}$ to be independent of k, we have $h_{\rm today} \propto a_{\rm entry}$. Horizon entry occurs when $a_{\rm entry} H_{\rm entry} = k$ and so from the scaling of H in matter and radiation domination we obtain $a_{\rm entry} \propto k^{-1}$ for radiation domination and $a_{\rm entry} \propto k^{-2}$ for matter domination. This gives the scalings

$$h \propto \begin{cases} 1 & k < 1/\tau_0 \\ k^{-2} & 1/\tau_0 < k < 1/\tau_{eq} \\ k^{-1} & 1/\tau_{eq} < k \end{cases} \tag{3.67}$$

For polarisation $X \in \{E, B\}$ we therefore expect since $k \sim l$ and $C_l^{XX} \sim (h')^2$ that

$$l(l+1)C_l^{XX} \propto \begin{cases} l^2 & l < l_R \\ l^{-2} & l_R < l < l_{eq} \\ 1 & l_{eq} < l < l_\Delta \\ l^{-4} & l_\Delta < l \end{cases} \tag{3.68}$$

which can be seen in the power spectra, clearly demonstrating the peak at l_R and the different scalings for modes entering in matter and radiation domination. We have introduced an additional scale l_Δ corresponding to the width of the SLS, above which the phase damping effect (described below) becomes important, leading to a suppression. Consequently, we don't see the constant scaling in the power spectrum.

3.3.2 Projection Factors

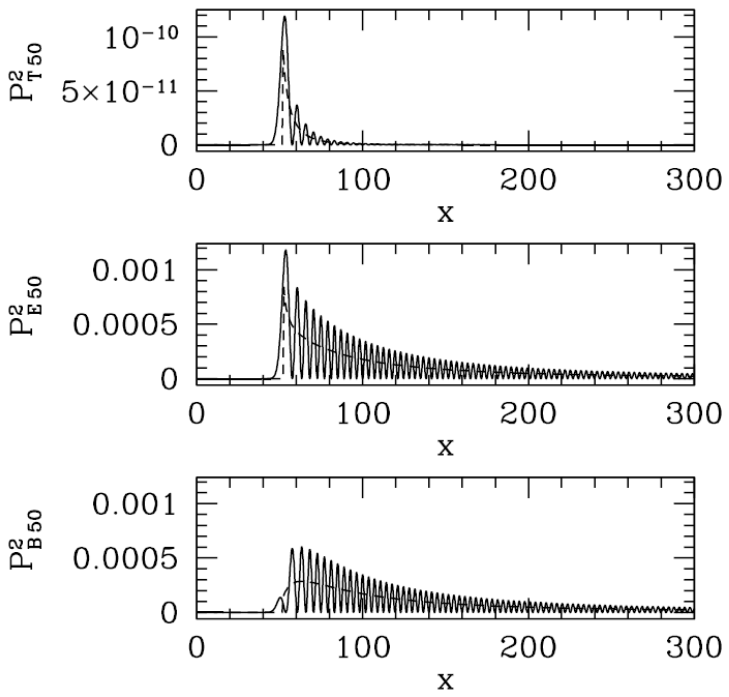

Figure 6. Squares of projection terms for $l = 50$. Dashed curve shows time averaged analytic approximations used.

When viewing the CMB we are viewing the projection of a 3D system onto a sphere. We can think of the weird looking spherical bessel like terms as projection factors, defining

$$P_{Tl}(x) = \frac{j_l(x)}{x^2} \tag{3.69}$$

$$P_{El}(x) = -j_l(x) + j_l''(x) + \frac{2j_l(x)}{x^2} + \frac{4j_l'(x)}{x} \tag{3.70}$$

$$P_{Bl}(x) = 2j_l'(x) + \frac{4j_l(x)}{x} \tag{3.71}$$

with argument $x = k(\tau_0 - \tau)$, the lookback time scaled by wavenumber. These are all peaked at $x \approx l$, i.e. C_l is dominated by the behaviour of the source at $x \approx l$. The polarisation source function is strongly peaked at $\tau = \tau_R$, implying $k \approx l/(\tau_0 - \tau_R)$ dominates the power spectrum. The departure of these projectors from a delta function, ie the large $x > l$ tail, indicates larger wave number modes also contribute to power at this angular scale, giving an overall smoothing to the power spectrum.

There exist several approximations for spherical bessel functions at $x \gg l$ and $x \ll l$, but unfortunately for our purposes we are interested in the peaks at $x \approx l$. Noticing the projection functions only really contribute for $x > l$ we may use the approximation valid for $x > l$

$$j_l(x) = \frac{1}{\sqrt{x^2 \sin\alpha}} \cos[x(\sin\alpha - \alpha\cos\alpha) - \pi/4] \tag{3.72}$$

with $\cos\alpha = (l + 1/2)/x$. This reduces to the more familiar $j_l(x) \approx \sin(x - l\pi/2)/x$ for $x \gg l$. In power spectra, these projection functions appear as squares, and their fast time oscillations aren't important. We may therefore time average, making use of the relations $\langle \sin^2 x \rangle = \langle \cos^2 x \rangle = 1/2$ and $\langle \sin x \cos x \rangle = 0$ to obtain explicit expressions. For instance,

$$\langle P_T(x)^2 \rangle \approx \frac{1}{2x^5\sqrt{x^2 - l^2}} \tag{3.73}$$

with similar more complicated expressions for E, B (plotted in figure 3.3.2). Note these diverge as $x \to l$, and so we must introduce an order unity cut-off a and restrict to the domain $x > l + a$

3.3.3 Source Evolution

One begins by expanding the Boltzmann equation 3.35 into an infinite 'heirachy' of moments. These may be numerically integrated time-step by time-step, up to some arbitrary large cut off l, which is the approach taken by codes. To make analytical progress, we employ the tight coupling approximation, in which higher order moments are suppressed by the scattering rate κ' being large during recombination. Each moment is smaller than the last by a factor of of κ', and so to leading order we may keep just

$$\begin{aligned} \tilde{\Delta}_{T0}' &= -h' - \kappa'[\tilde{\Delta}_{T0} - \Psi] \\ \tilde{\Delta}_{P0}' &= -\kappa'[\tilde{\Delta}_{T0} + \Psi] \\ \tilde{\Delta}_{Tl}' &= 0 \quad \text{for} \quad l \geq 1 \\ \tilde{\Delta}_{Pl}' &= 0 \quad \text{for} \quad l \geq 1 \end{aligned} \tag{3.74}$$

In this limit $\Psi = \frac{1}{10}\tilde{\Delta}_{T0} - \frac{3}{5}\tilde{\Delta}_{P0}$, and so combining the first two (continuity) equations we obtain

$$\Psi' + \frac{3}{10}\kappa'\Psi = -\frac{h'}{10} \tag{3.75}$$

Integrating,

$$\Psi(\tau) = -\int_0^\tau d\tau' \frac{h'(\tau')}{10} \exp\left(-\frac{3}{10}(\kappa(\tau') - \kappa(\tau))\right) \tag{3.76}$$

Now making the Gaussian approximation on the visibility function 3.39 we take $\kappa' \approx -\kappa/\Delta\tau_R$. Changing variable of integration to $x = \kappa(\tau')/\kappa(\tau)$ gives

$$\Psi(\tau) = -\frac{h'(\tau_R)}{10} e^{3\kappa(\tau)/10} \Delta\tau_R \int_1^\infty \frac{dx}{x} e^{-3\kappa(\tau)x/10} \tag{3.77}$$

In pulling the gravitational wave amplitude out of the integral we have assumed h varies slowly over the visibility function, an assumption only valid for modes $k \ll 1/\Delta\tau_R$. At larger wavenumbers h oscillates rapidly over the visibility function and so we may improve this by replacing $h'(\tau_R)$ with its time averaged value over the visibility function

$$\langle h'(\tau) \rangle = \int_0^\tau d\tau' g(\tau') h'(\tau') \approx h'(\tau_R) e^{-(k\Delta\tau_R)^2/2} \tag{3.78}$$

obtained through treating h' as purely oscillatory with a slowly varying envelope. Integrating an oscillatory function over a Gaussian leads to the function evaluated at its peak multiplied by an exponential suppression. This gives a small scale damping effect, akin to the diffusion damping encountered when considering scalar perturbations. In this context we term this phase damping - large k modes have contributions from many different regions in the SLS, each with a different phase. The net result is cancellation and a decrease and smoothing in observed power.

3.3.4 Analytic Power Spectra

Armed with an analytic solution for Ψ we proceed to compute the polarisation multipole generated. For $X \in \{E, B\}$ we have

$$\begin{aligned}
\Delta_{Xl} &= \int_0^{\tau_0} d\tau [-g\Psi P_{Xl}(k(\tau_0 - \tau))] \\
&\approx P_{Xl}(k(\tau_0 - \tau_R)) \int_0^{\tau_0} d\tau [-g\Psi] \\
&= P_{Xl}(k(\tau_0 - \tau_R)) \frac{h'(\tau_R)}{10} \Delta\tau_R e^{-(k\Delta\tau_R)^2/2} \int_0^\infty d\kappa e^{-7\kappa/10} \int_1^\infty \frac{dx}{x} e^{-3\kappa x/10} \\
&= P_{Xl}(k(\tau_0 - \tau_R)) h'(\tau_R) \Delta\tau_R e^{-(k\Delta\tau_R)^2/2} (\frac{1}{7} \log \frac{10}{3})
\end{aligned} \tag{3.79}$$

where, in the second line we pull the projection term outside the integral, assuming it varies slowly over the width of the visibility function. In the third line we convert from a conformal time to optical depth integral, and in the last line we have evaluated the integrals to $(10/7) \log 10/7$. From this we may calculate the polarisation power spectra

$$C_l^{XY} = (4\pi)^2 (\frac{1}{7} \log \frac{10}{3})^2 \int \frac{k^2 dk}{(2\pi)^3} P_t(k) P_{Xl}(k(\tau_0 - \tau_R)) P_{Yl}(k(\tau_0 - \tau_R)) h'_k(\tau_R)^2 (\Delta\tau_R)^2 e^{-(k\Delta\tau_R)^2} \tag{3.80}$$

We have analytic solutions to all of these quantities, which we proceed to plot in figure 7. For the B mode spectra of interest, we see the analytic solution is rather good for low l, the regime in which our assumptions are most valid. The key features of the spectrum are as follows. We have a peak at $l \approx 90$, corresponding to the horizon size at penultimate scattering. Analytically, this is firstly due to the projection terms being combinations of bessel functions $j_l(k(\tau_0 - \tau_R))$ peaking at $l \approx k(\tau_0 - \tau_R) \approx k\tau_0$. Then recalling in matter domination $h'(\tau_R) \sim j_2(k\tau_R)$, and using that $j_2(x)$ peaks at $x \approx 3$ we see a peak of h' at $k\tau_R = 3$, and so overall we have a peak at $l \approx k\tau_0 \approx 3\tau_0/\tau_R$. The height of this peak is controlled both by r, giving the amplitude of h and P_t, but also by the duration of last scattering, through the $\Delta\tau_R$ term. We get further peaks, due to the oscillatory behaviour of both the projection functions and h, which are suppressed by the phase damping effect, controlled by the width $\Delta\tau_R$ of the SLS.

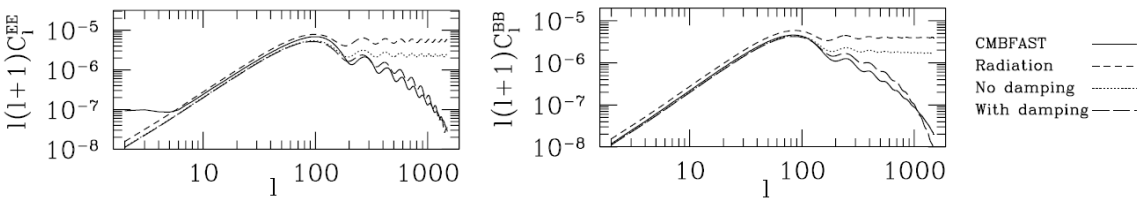

Figure 7. Comparison of E and B power spectra from CMBFAST (solid curve) with (semi)analytic approximations. The (semi)analytic solutions use forms for h in radiation domination, calculated numerically, and calculated numerically with exponential damping.

Throughout we have taken the visibility function to be near Gaussian, and peaked around recombination. We know however CMB photons scatter further at reionisation, which modifies the above discussion. Similarly to recombination, this contributes a peak at a new scale, that of the horizon size at reionisaton, to the polarisation power sepctra. Since the horizon is growing, this peak is at a larger angular scale contribution than the recombination peak, at $l < 10$. It also contributes a further exponential suppression at small scales [19].

Through carefully developing an analytic understanding of these power spectra, we have uncovered certain parameters and scales that can be probed provided a sufficiently precise measurement of the B mode spectrum. Tensor power spectra are sensitive to the following: the horizon scales at recombination and reionisation, the horizon scale at matter-radiation equality, the width of the SLS, among other cosmological parameters. In the near future we don't expect to be able to measure this full spectrum, and so for the purposes of this essay and for an initial measurement of r, the existence of the power spectrum peaks at fixed known l and predictable size given r is the key result.

3.4 Inflationary Density Perturbations

For completeness we should discuss scalar perturbations too. Importantly, these do not produce a B mode polarisation, a fact for which we give just some intuition for here, though one can perform an entirely analogous analysis for scalars also. As before, we work in Fourier space with wave vector $\mathbf{k}$, which we may choose to be aligned with the $\hat{\mathbf{z}}$ direction, and take the basis on which we evaluate Q and U along line of sight $\hat{\mathbf{n}}$ to be the natural basis on the sphere: $(\hat{\mathbf{e}}_1, \hat{\mathbf{e}}_2) = (\hat{\mathbf{e}}_\theta, \hat{\mathbf{e}}_\phi)$. Scalar perturbations are aligned with $\mathbf{k}$, and so the angular dependence of this system, and therefore of the Boltzmann equations too, turn out this time to only be in the dot product of the two relevant directions $\mu = \hat{\mathbf{k}} \cdot \hat{\mathbf{n}}$. Tensor perturbations on the other hand additionally had azimuthal dependence. The scalar quadrupole moment generated therefore has no ϕ dependence, i.e. is the $m = 0$ mode, and so generates azimuthally symmetric polarisation. Thus, recalling Q describes the difference in power between the $\hat{\mathbf{e}}_\theta$ and $\hat{\mathbf{e}}_\phi$ directions, we see Q is non zero as polarisation is aligned with $\hat{\mathbf{e}}_\theta$. U on the other hand is not, as it measures the difference of power between $\hat{\mathbf{e}}_\theta \pm \hat{\mathbf{e}}_\phi$, which are equal. Another way to say the same thing is that the polarisation eigenvector must be proportional to $\hat{\mathbf{e}}_\theta$, which by the form of the polarisation matrix forces $U = 0$. Now by 3.14, we see if $U = 0$, then $B(\hat{\mathbf{n}})$ is identically 0. One can think of the additional linearly independent degree of freedom in tensor perturbations being responsible for their azimuthal dependence, which results in both Q and U and so both E and B mode polarisation being generated.

4 Observing B Modes

We have seen that primordial perturbations induce characteristic polarisation patterns in the CMB. The significance of the E/B decomposition is now clear, since

1. Scalar (density) perturbations create only E modes, and no B modes
2. Vector (vorticity) perturbations create mainly B modes
3. Tensor (gravitational wave) perturbations create both E and B modes

In the previous section we showed (1) and (3). We omitted showing (2) since it can be shown that vector perturbations redshift away rapidly due to cosmic expansion, and so are not expected to contribute significantly to the observed B mode signal [20]. They all additionally source temperature anisotropies.

The B mode is therefore clearly special - theory tells us scalar perturbations do not produce it. This is the reason why searching for tensor perturbations in the B mode is significantly more promising than in the E mode or temperature isotropy. Tensors contribute to angular power spectra on large scales, where scalar contributions can be shown to be relatively small. Unfortunately, even in models predicting a large low l reionization or recombination feature, the overall power there is still too small to be measurable. For the E modes and temperature anistropies cosmic variance limits our ability to accurately measure the low l contribution of scalar perturbations, rendering it hard to unambiguously separate the scalar and tensor contributions. The B mode on the other hand is not contaminated by this cosmic variance prone scalar contribution, instead only limited by noise. In principle, with sufficient noise sensitivity, we can detect even very small tensor to scalar ratios in the low l regime [21]. There is a claim that a detection of B modes provides 'smoking-gun' evidence for primordial IGWs and therefore inflation [22], and so the search for these B modes is current major focus of observational cosmology - a detection will have far reaching consequences for the entire theoretical physics community.

Having motivated the search for B modes, we now turn to a number of issues in their detection. To be sure we have detected primordial gravitational waves, we must be sure a measured signal can only be attributed to them, not generated by some other effect. We discuss three points here, in varying levels of detail. Firstly, other possible sources of B modes in the early universe. Secondly, the issue of foregrounds: emission from other sources obscuring the CMB polarisation signal. Finally, and most interestingly, the weak gravitational lensing of CMB photons by intervening matter between us and the surface of last scattering. These issues, combined with the fact that the expected amplitude of B mode signal is tiny, makes their detection a daunting task.

4.1 Other Primordial B Modes

A number of other early universe effects are capable of producing B modes even in the absence of IGWs, and our analysis should account for the possibility that these contribute too. We use the illustrative example of topological defects, generically found in supersymettric grand unification models [2].

The best studied phenomena is that of cosmic strings, formed at the end of multi-field inflation upon the breaking of a $U(1)$ symmetry. If formed, they would induce a B mode polarisation in the CMB through continously sourced vector perturbations after inflation, no longer negligible as they havn't redshifted away by recombination or reionisation. They predict a spectrum with two peaks, at $l \approx 10$ from reionisation and $l \approx 600 - 1000$ from last-scattering. Recent work has found that topological defects alone cannot explain the measured BICEP-2 B mode signal, though may be present in combination with tensor or dust contributions [23].

Other primordial B modes may be generated by phase transitions [24] or primordial magnetic fields [25], each with their own characteristic spectra.

4.2 Foregrounds

Unfortunately, spread out between us and the last-scattering surface at $z \approx 1100$, there is a long line of obtruding foregrounds that hinder our ability to accurately measure the CMB fields. In this brief section we give an overview of the main foregrounds that contaminate our CMB polarisation signal, and describe how we may go about dealing with them. We draw from [26] and [27].

Recall first that the CMB is a near perfect black body emitter, with a characteristic frequency profile given by the Planck distribution peaking at about 160Ghz, see figure 8. Foregrounds can broadly be separated into three classes: time dependent atmospheric noise, galactic, or extragalactic. Each individual type of foreground has its own distinctive frequency dependence, and degree of polarisation. Those contributing at CMB frequencies are summarised in figure 9. We see the main astrophysical contaminants for our studies of polarisation are galactic in origin, from synchrotron emission at low frequencies below 100Ghz, and thermal dust at higher frequencies, rendering the entire galactic plane virtually unusable for CMB measurements. The other contaminants listed in the left panel turn out to not be significantly polarised so don't pose too much of an issue. The right panel demonstrates the extent of the problem - the expected B mode signal, even for a relatively large value of $r \approx 0.1$ falls below the average polarised foreground level on the full sky at all CMB frequencies.

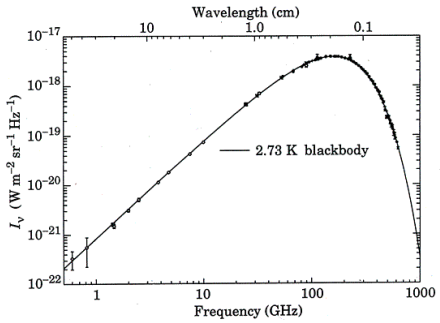

Figure 8. The CMB spectrum as measured by the COBE sattelite, matches that of a black body emitter at the CMB temperature. Figure from https://webhome.phy.duke.edu/ kolena/cmb.html.

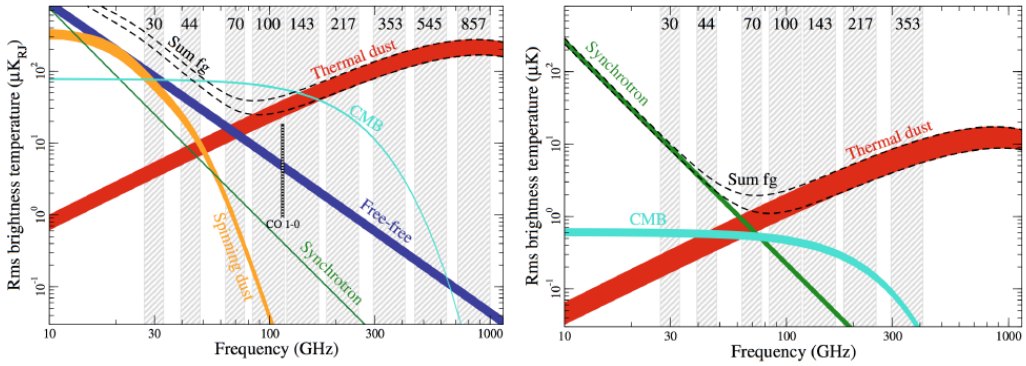

Figure 9. Spectral energy distributions (SEDs) of relevant astrophysical foregrounds. The left panel are the main contributions to temperature, and the right, to polarisation. The shaded bars indicate the observation frequencies for the Planck satellite, and the upper and lower limits correspond to different galactic masks obscuring 7 and 19% of the sky, primarily in the galactic plane. Figure from [28].

Atomospheric effects: Absorption lines from oxygen at 60 and 120 Ghz, and water vapour at 18 and 20Ghz limit access to the microwave sky. Thermal emission from the atmosphere is unpolarised,

though Zeeman splitting of oxygen lines in Earth's magnetic field gives primarily circularly polarized emission. While the CMB is not expected to be circularly polarized, instrumental issues could lead to a $\approx 0.01\%$ circular-to-linear polarisation conversion, which could still give a measured B mode signal orders of magnitude larger than if $r = 0.01$, say. Backscattering of thermal radiation emitted by the earth's surface off ice crystal clouds in the troposphere may also give B mode signals larger than the expected CMB B mode signal.

Galactic Synchrotron: This emission is produced by acceleration of charged particles in interstellar magnetic fields. Via multi frequency measurements from the WMAP and Planck satellites, we find a very good fit to spectral energy distribution $T_d(\nu) \propto \nu^{\beta_s}$ with $\beta_s \approx -3$ but varying slightly over the sky, due to the dependence on the acceleration of charged particles.

Galactic Dust: This emission is produced due to presence of dust grains in the interstellar medium. In dense regions of star formation, UV radiation from newly formed stars heats up nearby dust, which radiate strongly polarised light in the IR and microwave frequencies. The grain size and dust temperature determine the spectral properties of the radiation, which can be fitted well to a modified black body emission spectrum $T_d(\nu) \propto \nu^{\beta_d+1}[e^{\nu/T} - 1]^{-1}$. Measurements from Planck show T_d and spectral parameter β_d vary over the sky, with average values differing significantly in and out of the galactic plane. While no region of the sky was found to be sufficiently clean of dust to require no foreground removal for clean B mode measurements, Planck did identify certain patches of the sky with considerably lower foreground amplitudes, which may be of use in future CMB missions.

The statistical algorithms and methods designed to separate these foregrounds from the clean CMB (the primary signal plus secondary effects) are known as CMB component separation [29], and make use of several datasets. They can be grouped into two classes. Non blind methods attempt to make use of the known spectral frequency properties of certain foregrounds, while blind methods assume little or no prior information about the form of the foregrounds, instead relying on their statistics: different foregrounds should be statistically independent, and the statistics of the primary CMB are well understood from theory.

Proper foreground removal is very important. In order to detect a B mode signal from $r = 0.01$ IGWs at a 3σ significance for example, we must only have a 1% level of residual foregrounds. It is however easy to go wrong. In March 2014 the BICEP2 Collaboration reported detection of B mode power at 150 GHz in the range $40 < l < 100$, in excess of that expected from lensing (see next section), and greater than that expected from foregrounds [30]. This would have been huge, even making public news [22]. However unfortunately, under further scrutiny, arguments were made that uncertainties in the various dust templates may have been underestimated. By cross correlating with newer BICEP2/Keck and Planck data it was found that this entire excess B mode could be attributed to dust, leaving again only an improved upper bound on r [31].

4.3 CMB Lensing

CMB lensing is the deflection of CMB photons by all intervening matter in the universe by gravity. It is a second order effect and is thus not treated in the linearised Boltzmann equation formalism used to describe the CMB so far. While in the linear regime each Fourier mode evolves independently, lensing mixing these Fourier modes, making the statistics of the lensed sky far more complicated than those of the unlensed one.

We treat lensing in the 'weak lensing' regime, where images (and also generally other fields on the sphere) experience a small shift compared to the original unlensed field. The effect of gravitational lensing is greatest when the lens (i.e. the matter responsible for the deflection) is massive, and close to the source. While some lenses for the CMB are certainly massive, they are relatively far from the $z \approx 1100$ source, since structure doesn't form in the universe until a much later time. The opposing

'strong lensing' regime is also very interesting for cosmology, though not relevant here.

Lensing affects all three of our observable CMB fields: the temperature fluctuation T, and Stokes parameters Q and U, and in doing so also the derived physical E and B fields in a way that will be made precise later. It has the effect of locally (i.e. on small patches of the sky) sqaushing and stretching the CMB, shifting local power spectra towards lower or higher angular scales. Summing over many patches we see a small smoothing of oscillations in the temperature and E mode spectra at a measurable several percent, rendering the effect important in precision cosmology.

Importantly, it also has the effect of converting some primordial E modes into lensed B modes, which we demonstrate and quantify in the flat sky limit. This obscures the inflationary B mode signal, and so lensing acts as a nuisance for our studies of the primary CMB. It is not all bad however - a typical analysis of the CMB assumes Gaussianity and statistical isotropy, giving us just a power spectrum. Lensing introduces small amounts of non-Gaussianity and statistical anisotropy into the CMB, so can be thought of as adding information to the CMB which may be used to probe the matter distribution of the universe at out to further redshifts than possible with current galaxy surveys [32].

4.3.1 Mathematical Description

The mathematical formalism used to describe lensing for our purposes is rather simple, and described in great detail in [9], on which much of this section is based. From General Relativity and a flat FLRW metric, one can derive an expression for the displacement vector $\boldsymbol{\alpha}$ on the sphere, dependent on observed direction $\hat{\mathbf{n}}$, by which the lensed and unlensed fields differ.

$$\tilde{X}(\hat{\mathbf{n}}) = X(\hat{\mathbf{n}} + \boldsymbol{\alpha}) \tag{4.1}$$

$$\boldsymbol{\alpha} = -2\int_0^{\chi_*} d\chi \frac{\chi_* - \chi}{\chi_* \chi} \nabla_{\hat{\mathbf{n}}} \Psi(\chi\hat{\mathbf{n}}, \tau_0 - \chi) \tag{4.2}$$

Throughout this section a tilde indicates a lensed field, not to be confused with how we defined $\tilde{E}$ and $\tilde{B}$ previously. $X \in \{T, U, V\}$ is an observable field, χ is conformal distance, $\tau_0 - \chi$ is the conformal time at which the photon was at position $\chi\hat{\mathbf{n}}$, $\nabla_{\hat{\mathbf{n}}}$ is the angular derivative, or equivalently covariant derivative on the sphere, and $\Psi = \frac{1}{2}(\Psi_N + \Phi_N)$ is the Weyl potential, written in terms of the Newtonian potentials 2.14. We have used here the Born approximation - the line of sight integral is performed along the unperturbed geodesic path, valid as we work to first order in Ψ, which has been shown to be a very good approximation. Ψ is related to matter perturbations by the Poisson Equation

$$\nabla^2 \Psi = 4\pi G \bar{\delta\rho} \tag{4.3}$$

where $\bar{\delta\rho}$ is the comoving total density perturbation, i.e. evaluated in its rest frame, and we have assumed no anisotropic stress. It is convenient to write the deflection angle instead in terms of a lensing potential

$$\begin{aligned} \psi(\hat{\mathbf{n}}) &= -2\int_0^{\chi_*} d\chi \frac{\chi_* - \chi}{\chi_* \chi} \Psi(\chi\hat{\mathbf{n}}, \tau_0 - \chi) \\ \boldsymbol{\alpha} &= \nabla\psi \end{aligned} \tag{4.4}$$

One may worry about the lensing potential being divergent as $\chi \to 0$. We can amend this by setting the monopole of ψ to 0, which doesn't modify $\boldsymbol{\alpha}$.

4.3.2 Lensing Potential Power Spectrum

We ultimately wish to calculate the lensed power spectra in terms of the unlensed. In doing so, we will need the lensing potential power spectrum. Here we derive an expression for it, showing it is simply a weighted matter power spectrum. We make use of the Fourier space expression

$$\langle \Psi(\mathbf{k}, \tau, \tau') \Psi^*(\mathbf{k}', \tau, \tau') \rangle = (2\pi)^3 \delta(\mathbf{k} - \mathbf{k}') \frac{2\pi^2}{k^3} \Delta^2_\Psi(k, \tau, \tau') \tag{4.5}$$

to get

$$\begin{aligned}\langle\psi(\hat{\mathbf{n}})\psi(\hat{\mathbf{n}}')\rangle &= 4\int d\chi\int d\chi'(\frac{\chi_*-\chi}{\chi_*\chi})(\frac{\chi_*-\chi'}{\chi_*\chi'})\int\frac{d^3\mathbf{k}}{(2\pi)^3}\frac{2\pi^2}{k^3}\Delta^2_\Psi(k,\tau,\tau')e^{i\mathbf{k}\cdot\mathbf{x}}e^{-i\mathbf{k}\cdot\mathbf{x}'}\\ &= 16\pi\sum_{ll'mm'}\int d\chi\int d\chi'(\frac{\chi_*-\chi}{\chi_*\chi})(\frac{\chi_*-\chi'}{\chi_*\chi'})\int\frac{dk}{k}j_l(k\chi)j_{l'}(k\chi')Y_{lm}(\hat{\mathbf{n}})Y^*_{l'm'}(\hat{\mathbf{n}}')\delta_{ll'}\delta_{mm'}\end{aligned} \tag{4.6}$$

where we have made use of the Rayleigh plane wave identity with $\mathbf{x}=\chi\hat{\mathbf{n}}$

$$e^{i\mathbf{k}\cdot\mathbf{x}} = 4\pi\sum_{lm} i^l j_l(k\chi)Y^*_{lm}(\hat{\mathbf{n}})Y_{lm}(\hat{\mathbf{k}}) \tag{4.7}$$

and performed the angular $\hat{\mathbf{k}}$ integral using orthogonality of spherical harmonics. Finally we expand

$$\psi(\hat{\mathbf{n}}) = \sum_{lm}\psi_{lm}Y_{lm}(\hat{\mathbf{n}}) \tag{4.8}$$

and recalling the definition of $C_l^{\psi\psi}$

$$\langle\psi_{lm}\psi^*_{l'm'}\rangle = C_l^{\psi\psi}\delta_{ll'}\delta_{mm'} \tag{4.9}$$

read off the angular power spectrum

$$C_l^{\psi\psi} = 16\pi\int_0^{\chi_*}d\chi\int_0^{\chi_*}d\chi'\int\frac{dk}{k}(\frac{\chi_*-\chi}{\chi_*\chi})(\frac{\chi_*-\chi'}{\chi_*\chi'})j_l(k\chi)j_l(k\chi')\Delta^2_\Psi(k,\tau_0-\chi,\tau_0-\chi') \tag{4.10}$$

To make the relation with scalar perturbations explicit, we may relate this to primordial perturbations via a transfer function $\Psi(\mathbf{k},\tau)=T_\Psi(k,\tau)\zeta(\mathbf{k})$, giving

$$C_l^{\psi\psi} = 16\pi\int\frac{dk}{k}P_s(k)\left[\int_0^{\chi_*}d\chi j_l(\chi)(\frac{\chi_*-\chi}{\chi_*\chi})T_\Psi(k,\tau_0-\chi)\right]^2 \tag{4.11}$$

Alternatively, we may relate the scale invariant power spectrum of Ψ to the conventionally defined matter power spectrum via Fourier transforming the Poisson Equation 4.3, making concrete the claim the lensing potential power spectrum is a weighted matter power spectrum.

$$\Delta^2_\Psi(k,\tau) = \frac{9\Omega_m^2(\tau)H^4(\tau)}{8\pi^2}\frac{P_m(k,\tau)}{k} \tag{4.12}$$

4.3.3 Lensing of B modes

We now calculate in the flat sky regime, the effect lensing has on temperature, E mode, and importantly, B mode power spectra. We start with temperature, and will see the polarisation calculations following similarly. We use here the series expansion approach, which gives good intuition and qualitatively correct results, though is not a good approximation on all scales. A more accurate approach instead works with real space correlation functions directly. Expanding,

$$\tilde{T}(\hat{\mathbf{n}}) = T(\hat{\mathbf{n}}+\nabla\psi) = T(\hat{\mathbf{n}}) + \nabla^a\psi(\hat{\mathbf{n}})\nabla_a T(\hat{\mathbf{n}}) + \frac{1}{2}\nabla^a\psi(\hat{\mathbf{n}})\nabla^b\psi(\hat{\mathbf{n}})\nabla_a\nabla_b T(\hat{\mathbf{n}}) + O(\psi^3) \tag{4.13}$$

Fourier transforming and using the convolution theorem we obtain

$$\begin{aligned}\tilde{T}(\mathbf{l}) &= T(\mathbf{l}) - \int\frac{d^2\mathbf{l_1}}{(2\pi)^2}\mathbf{l_1}\cdot(\mathbf{l}-\mathbf{l_1})T(\mathbf{l_1})\psi(\mathbf{l}-\mathbf{l_1})\\ &\quad - \frac{1}{2}\int\frac{d^2\mathbf{l_1}}{(2\pi)^2}\int\frac{d^2\mathbf{l_2}}{(2\pi)^2}\mathbf{l_1}\cdot(\mathbf{l_1}+\mathbf{l_2}-\mathbf{l})\mathbf{l_1}\cdot\mathbf{l_2}T(\mathbf{l_1})\psi(\mathbf{l_2})\psi^*(\mathbf{l_1}+\mathbf{l_2}-\mathbf{l})\\ &= T(\mathbf{l}) - \int\frac{d^2\mathbf{l_1}}{(2\pi)^2}T(\mathbf{l_1})L(\mathbf{l},\mathbf{l_1})\end{aligned} \tag{4.14}$$

making use of $\psi(\mathbf{l}) = \psi^*(-\mathbf{l})$, and where we have defined

$$L(\mathbf{l}, \mathbf{l_1}) = \mathbf{l_1} \cdot (\mathbf{l} - \mathbf{l_1})\psi(\mathbf{l} - \mathbf{l_1}) + \frac{1}{2}\int \frac{d^2\mathbf{l_2}}{(2\pi)^2}\mathbf{l_1} \cdot (\mathbf{l_1} + \mathbf{l_2} - \mathbf{l})\mathbf{l_1} \cdot \mathbf{l_2}\psi(\mathbf{l_2})\psi^*(\mathbf{l_1} + \mathbf{l_2} - \mathbf{l}) \tag{4.15}$$

Now in the flat sky limit the appropriate definition of the (lensed) regular power spectrum of fourier modes is

$$\langle T^*(\mathbf{l})T(\mathbf{l}')\rangle = (2\pi)^2\delta(\mathbf{l} - \mathbf{l}')C_l^{TT} \tag{4.16}$$

where we choose to retain the notation C_l here. To lowest order in the lensing potential power spectrum, we may calculate using Wick's theorem and the fact that T and ψ don't correlate

$$\begin{aligned}\tilde{C}_l^{TT} &\approx C_l^{TT} + \int \frac{d^2\mathbf{l_1}}{(2\pi)^2}[\mathbf{l_1} \cdot (\mathbf{l} - \mathbf{l_1})]^2 C^{\psi}_{|\mathbf{l}-\mathbf{l_1}|}C^{TT}_{l_1} - C_l^{TT}\int \frac{d^2\mathbf{l_1}}{(2\pi)^2}[\mathbf{l} \cdot \mathbf{l_1}]^2 C^{\psi\psi}_{l_1} \\ &= (1 - l^2R^{\psi})C_l^{TT} + \int \frac{d^2\mathbf{l_1}}{(2\pi)^2}[\mathbf{l_1} \cdot (\mathbf{l} - \mathbf{l_1})]^2 C^{\psi}_{|\mathbf{l}-\mathbf{l_1}|}C^{TT}_{l_1}\end{aligned} \tag{4.17}$$

where

$$R^{\psi} = \frac{1}{4\pi}\int \frac{dl}{l} l^4 C_l^{\psi\psi} \tag{4.18}$$

For polarisation, the calculation is rather similar. Recall that in the flat sky limit we must rotate Q and U Fourier modes into E and B modes as 3.31

$$\begin{aligned}P_{\pm}(\hat{\mathbf{n}}) := (Q \pm iU)(\hat{\mathbf{n}}) &= \int \frac{d^2\mathbf{l}}{(2\pi)^2}(E(\mathbf{l}) \pm iB(\mathbf{l}))e^{\pm 2i\phi_{\mathbf{l}}}e^{i\mathbf{l}\cdot\hat{\mathbf{n}}} \\ \Leftrightarrow P_{\pm}(\mathbf{l}) &= (E(\mathbf{l}) \pm iB(\mathbf{l}))e^{\pm 2i\phi_{\mathbf{l}}}\end{aligned} \tag{4.19}$$

Now lensing acts on $P_{\pm}$ exactly as it did on the temperature field

$$\tilde{P}_{\pm}(\hat{\mathbf{n}}) = P_{\pm}(\hat{\mathbf{n}} + \nabla\psi) = P_{\pm}(\hat{\mathbf{n}}) + \nabla^a\psi(\hat{\mathbf{n}})\nabla_a P_{\pm}(\hat{\mathbf{n}}) + \frac{1}{2}\nabla^a\psi(\hat{\mathbf{n}})\nabla^b\psi(\hat{\mathbf{n}})\nabla_a\nabla_b P_{\pm}(\hat{\mathbf{n}}) + O(\psi^3) \tag{4.20}$$

which in Fourier space gives

$$\tilde{P}_{\pm}(\mathbf{l}) \approx P_{\pm}(\mathbf{l}) - \int \frac{d^2\mathbf{l_1}}{(2\pi)^2}P_{\pm}(\mathbf{l_1})L(\mathbf{l}, \mathbf{l_1}) \tag{4.21}$$

Finally we use the relationship 4.19 between $P_{\pm}$ and E and B modes twice

$$\begin{aligned}\tilde{E}(\mathbf{l}) \pm i\tilde{B}(\mathbf{l}) &= e^{\mp 2i\phi_{\mathbf{l}}}\tilde{P}_{\pm}(\mathbf{l}) \\ &= e^{\mp 2i\phi_{\mathbf{l}}}\left(P_{\pm}(\mathbf{l}) - \int \frac{d^2\mathbf{l_1}}{(2\pi)^2}P_{\pm}(\mathbf{l_1})L(\mathbf{l}, \mathbf{l_1})\right) \\ &= E(\mathbf{l}) \pm iB(\mathbf{l}) - \int \frac{d^2\mathbf{l_1}}{(2\pi)^2}e^{\pm 2i(\phi_{\mathbf{l_1}} - \phi_{\mathbf{l}})}(E(\mathbf{l_1}) \pm iB(\mathbf{l_1}))L(\mathbf{l}, \mathbf{l_1})\end{aligned} \tag{4.22}$$

departing from the temperature case in this phase factor. Now we may calculate lensed power spectra involving polarisation fields

$$\langle E^*(\mathbf{l})E(\mathbf{l}')\rangle = (2\pi)^2\delta(\mathbf{l} - \mathbf{l}')C_l^{EE} \qquad \langle B^*(\mathbf{l})B(\mathbf{l}')\rangle = (2\pi)^2\delta(\mathbf{l} - \mathbf{l}')C_l^{BB} \tag{4.23}$$

and also C_l^{TE} omitted. Schematically, this calculation is similar to that for lensed temperature perturbations, and we pick up identical terms. By correlating $\tilde{E}(\mathbf{l}) \pm i\tilde{B}(\mathbf{l})$ with itself and $\tilde{E}(\mathbf{l}) \mp i\tilde{B}(\mathbf{l})$

we obtain

$$\begin{aligned}
\tilde{C}_l^{EE} + \tilde{C}_l^{BB} &\approx C_l^{EE} + C_l^{BB} + \int \frac{d^2\mathbf{l_1}}{(2\pi)^2}[\mathbf{l_1}\cdot(\mathbf{l}-\mathbf{l_1})]^2 C^{\psi}_{|\mathbf{l}-\mathbf{l_1}|}(C_{l_1}^{EE}+C_{l_1}^{BB}) \\
&\quad - (C_l^{EE}+C_l^{BB})\int \frac{d^2\mathbf{l_1}}{(2\pi)^2}[\mathbf{l}\cdot\mathbf{l_1}]^2 C_{l_1}^{\psi\psi} \\
\tilde{C}_l^{EE} - \tilde{C}_l^{BB} &\approx C_l^{EE} - C_l^{BB} + \int \frac{d^2\mathbf{l_1}}{(2\pi)^2} e^{4i(\phi_{\mathbf{l_1}}-\phi_{\mathbf{l}})}[\mathbf{l_1}\cdot(\mathbf{l}-\mathbf{l_1})]^2 C^{\psi}_{|\mathbf{l}-\mathbf{l_1}|}(C_{l_1}^{EE}-C_{l_1}^{BB}) \\
&\quad - (C_l^{EE}-C_l^{BB})\int \frac{d^2\mathbf{l_1}}{(2\pi)^2}[\mathbf{l}\cdot\mathbf{l_1}]^2 C_{l_1}^{\psi\psi}
\end{aligned} \tag{4.24}$$

The integrals are actually all real by symmetry in $\mathbf{l_1}$, and so we may replace the exponentials by cosines. Adding and subtracting we get

$$\begin{aligned}
\tilde{C}_l^{EE} &= (1-l^2R^{\psi})C_l^{EE} + \frac{1}{2}\int \frac{d^2\mathbf{l_1}}{(2\pi)^2}[\mathbf{l_1}\cdot(\mathbf{l}-\mathbf{l_1})]^2 C^{\psi}_{|\mathbf{l}-\mathbf{l_1}|} \\
&\quad \times [(C_{l_1}^{EE}+C_{l_1}^{BB}) + \cos 4(\phi_{\mathbf{l_1}}-\phi_{\mathbf{l}})(C_{l_1}^{EE}-C_{l_1}^{BB})] \\
\tilde{C}_l^{BB} &= (1-l^2R^{\psi})C_l^{BB} + \frac{1}{2}\int \frac{d^2\mathbf{l_1}}{(2\pi)^2}[\mathbf{l_1}\cdot(\mathbf{l}-\mathbf{l_1})]^2 C^{\psi}_{|\mathbf{l}-\mathbf{l_1}|} \\
&\quad \times [(C_{l_1}^{EE}+C_{l_1}^{BB}) - \cos 4(\phi_{\mathbf{l_1}}-\phi_{\mathbf{l}})(C_{l_1}^{EE}-C_{l_1}^{BB})]
\end{aligned} \tag{4.25}$$

Here comes the key point: even if C_l^{BB} is zero, i.e. the unlensed field has no B modes from IGWs, lensing creates some. This has important consequences for the detectability of B modes, which we expect to be small anyway.

We saw tensor mode spectra peak on large angular scales $l < 200$ so we seek to understand lensing B modes in that range. Taking $C_l^{BB} = 0$ we find for $|\mathbf{l}| \ll |\mathbf{l_1}|$ that

$$\begin{aligned}
\tilde{C}_l^{BB} &= \frac{1}{2}\int \frac{d^2\mathbf{l_1}}{(2\pi)^2}[\mathbf{l_1}\cdot(\mathbf{l}-\mathbf{l_1})]^2 C^{\psi}_{|\mathbf{l}-\mathbf{l_1}|} C_{l_1}^{EE}\sin^2 2(\phi_{\mathbf{l_1}}-\phi_{\mathbf{l}}) \\
&\approx \frac{1}{2}\int \frac{d^2\mathbf{l_1}}{(2\pi)^2} l_1^4 C_{l_1}^{\psi\psi} C_{l_1}^{EE}\sin^2 2(\phi_{\mathbf{l_1}}-\phi_{\mathbf{l}}) \\
&= \frac{1}{4\pi}\int \frac{dl_1}{l_1} l_1^6 C_{l_1}^{\psi\psi} C_{l_1}^{EE}
\end{aligned} \tag{4.26}$$

independent of l. This corresponds to a white noise spectrum independent of l for small l, a very good approximation for roughly $l \ll 1000$, the range over which we would want to observe B modes. The power spectra of ψ is related to the matter power spectrum and is well understood. The power spectrum of unlensed E is approximately the measured lensed E, and can also be predicted from theory assuming it is sourced primarily from scalar perturbations. These suffice to give a good approximation for the size of this white noise effect: $\tilde{C}_l^{BB} \approx 2\times 10^{-6}\mu K^2$, corresponding to an instrumental white-noise level of $\approx 5\mu$K-arcmin.

We are now in a position to demonstrate how large a problem lensing is. Figure 10 plots the power spectrum of B modes from IGWs for various values of r. It also plots the power of lensed B modes over the region we expect to see an inflationary B mode signal. We see the lensing contribution heavily obscures IGW B modes, though for r sufficiently large: i.e. within roughly an order of magnitude of the current upper bound, the reionisation and recombination peaks may may still stand out. Several experiments have confirmed detection of these lensing B modes in the range $200 < l < 1500$, for example first in 2014 by the POLARBEAR collaboration [34]. Shown also on the figure is an ambitious delensed signal, which we discuss next.

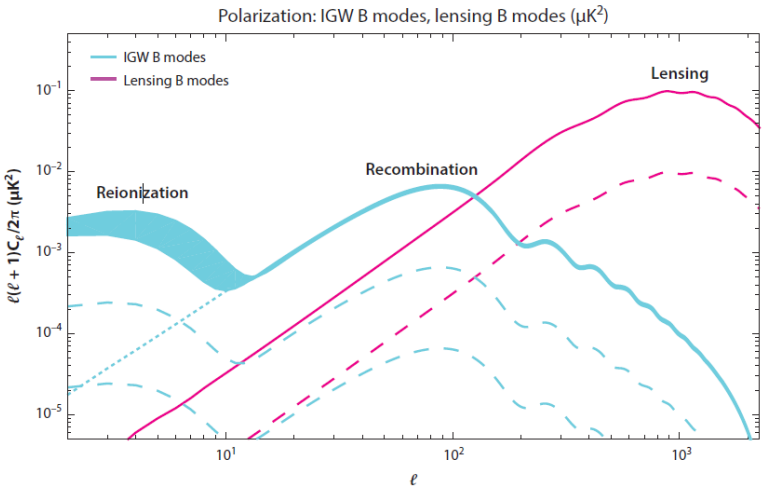

Figure 10. Polarisation power. Spectra are shown for IGW B modes with $r = \{0.1, 0.01, 0.001\}$ in cyan, and lensing induced B modes in magenta. We show here the reionisation feature omitted in the previous discussion, with $\pm 1\sigma$ uncertainity due to the current constraint on the optical depth to reionization shown only for $r = 0.1$. The cyan dotted line is the result with no reionization. A 90% delensed signal is shown in dotted magenta. Plots generated using CAMB [33], and taken from [13].

4.3.4 Delensing

In the limit of small instrumental noise, the dominant source of B mode power on large angular scales is gravitational lensing. For instrumental noise levels falling below the lensing white noise experiments will be lensing-limited: the limiting factor in constraining r will be the lensing B mode. While foregrounds can be removed through exploiting multifrequency data, this is not possible for lensing. Instead, delensing algorithms have been proposed which statistically separate the gravitational wave and lensing B mode signals, offering the prospect for reducing the noise floor and unlocking more modes for observation. These algorithms are based on a relatively simple idea: given information about noisy observed E modes, together with information about the lensing potential and therefore the deflection field, we can estimate the large-scale lensing B mode and subtract it from the observed B mode.

The required estimate for the defection field can be any probe of the universes matter distribution and may be obtained externally or internally. A promising external probe is the cosmic IR background, emitted by UV heated dust surrounding early stars, due to its high degree of correlation with the lensing signal [35]. Typically however an internal estimate is used, i.e. from the CMB itself, and we give an example of one such estimator in the next section.

Given an such an estimator $\hat{\psi}(\mathbf{l})$, we may use the lensed E mode as a proxy for the unlensed E mode, and write, via taking the imaginary part of 4.22

$$B^{\text{reconstructed}}(\mathbf{l}) = \int \frac{d^2\mathbf{l_1}}{(2\pi)^2} \mathbf{l_1} \cdot (\mathbf{l} - \mathbf{l_1}) \tilde{E}(\mathbf{l_1}) \hat{\psi}(\mathbf{l} - \mathbf{l_1}) \sin[2(\phi_{\mathbf{l_1}} - \phi_{\mathbf{l}})] \tag{4.27}$$

which we then subtract off of our observed B mode to get a delensed B mode

$$B^{\text{delensed}}(\mathbf{l}) = B^{\text{observed}}(\mathbf{l}) - B^{\text{reconstructed}}(\mathbf{l}) \tag{4.28}$$

The degree to which the B mode signal can be delensed ultimately depends on how well the reconstruction of ψ can be accomplished.

4.3.5 Lensing Reconstruction

The step we brushed under the rug above was the reconstruction of the lensing potential. Here we discuss the simplest of such estimators as in [9, 36], which have recently been used to create lensing mass maps over large portions of the sky by the ACT collaboration [37].

The idea here is that the unlensed CMB is statistically very simple - it is Gaussian, i.e. distinct Fourier modes are statistically independent: $\langle X^*(\mathbf{l})X(\mathbf{l}')\rangle = 0$ for $\mathbf{l} \neq \mathbf{l}'$. Lensing, being a non linear effect mixes these Fourier modes: we saw above by the convolution theorem that $\tilde{X}(\mathbf{l})$ picks up contributions from all modes $X(\mathbf{l_1})$ and $\phi(\mathbf{l_2})$ with $\mathbf{l_1} + \mathbf{l_2} = \mathbf{l}$. It thus contains information about the lensing potential.

Let us demonstrate this explicitly for the case of temperature perturbations. From the expression 4.14 we calculate the average over many CMB

$$\begin{aligned}\langle \tilde{T}(\mathbf{l})\tilde{T}^*(\mathbf{l}-\mathbf{L})\rangle &= \delta(\mathbf{L})C_l^{TT} - \int \frac{d^2\mathbf{l_1}}{(2\pi)^2}\mathbf{l_1}\cdot(\mathbf{l}-\mathbf{l_1})\psi(\mathbf{l}-\mathbf{l_1})\langle T(\mathbf{l_1})T^*(\mathbf{l}-\mathbf{L})\rangle \\ &\quad + \mathbf{l_1}\cdot(\mathbf{l}-\mathbf{L}-\mathbf{l_1})\psi^*(\mathbf{l}-\mathbf{L}-\mathbf{l_1})\langle T(\mathbf{l})T^*(\mathbf{l_1})\rangle + O(\psi^2) \\ &= \delta(\mathbf{L})C_l^{TT} + [(\mathbf{L}-\mathbf{l})\cdot\mathbf{L}C^{TT}_{|\mathbf{l}-\mathbf{L}|} + \mathbf{l}\cdot\mathbf{L}C_l^{TT}]\psi(\mathbf{l}) + O(\psi^2)\end{aligned} \tag{4.29}$$

The $\mathbf{L} \neq 0$ cross correlations therefore probe the lensing potential. To estimate the lensing potential we perform a weighted average of all off diagonal terms

$$\hat{\psi}(\mathbf{L}) = N(\mathbf{L})\int \frac{d^2\mathbf{l}}{(2\pi)^2}\tilde{T}(\mathbf{l})\tilde{T}^*(\mathbf{l}-\mathbf{L})g(\mathbf{l},\mathbf{L}) \tag{4.30}$$

where $g(\mathbf{l},\mathbf{L})$ is some weighting function and $N(\mathbf{L})$ some normalisation. To be unbiased at lowest order we want $\langle\hat{\psi}(\mathbf{L})\rangle = \psi(\mathbf{L})$, which by the previous calculation gives

$$N(\mathbf{L})^{-1} = \int \frac{d^2\mathbf{l}}{(2\pi)^2}[(\mathbf{L}-\mathbf{l})\cdot\mathbf{L}C^{TT}_{|\mathbf{l}-\mathbf{L}|} + \mathbf{l}\cdot\mathbf{L}C_l^{TT}]g(\mathbf{l},\mathbf{L}) \tag{4.31}$$

We now choose g to maximise the signal to noise. One can compute the variance to zeroth order in $C_l^{\psi\psi}$ as $\langle|\hat{\psi}(\mathbf{L}) - \psi(\mathbf{L})|^2\rangle \approx \langle|\hat{\psi}(\mathbf{L})|^2\rangle$ as

$$\langle\hat{\psi}^*(\mathbf{L})\hat{\psi}(\mathbf{L})\rangle = \delta(\mathbf{0})2N(\mathbf{L})^2\int\frac{d^2\mathbf{l}}{(2\pi)^2}\tilde{C}_l^{tot}\tilde{C}^{tot}_{|\mathbf{l}-\mathbf{L}|}g(\mathbf{l},\mathbf{L})^2 + O(C_l^{\psi\psi}) \tag{4.32}$$

where $\tilde{C}_l^{tot} = \tilde{C}_l^{TT} + N_l$ is the total observed lensed and noise spectrum. $\delta(\mathbf{0}) = f_{\rm sky}/\pi$ is interpreted in terms of sky area, often smaller than the full sky by use of a galactic mask. By differentiating this variance with respect to g, we may minimize the variance to 0th order via the choice

$$g(\mathbf{l},\mathbf{L}) = \frac{[(\mathbf{L}-\mathbf{l})\cdot\mathbf{L}C^{TT}_{|\mathbf{l}-\mathbf{L}|} + \mathbf{l}\cdot\mathbf{L}C_l^{TT}]}{2\tilde{C}_l^{tot}\tilde{C}^{tot}_{|\mathbf{l}-\mathbf{L}|}} \tag{4.33}$$

completing the construction of the minimum variance estimator

$$\hat{\psi}(\mathbf{L}) = N(\mathbf{l})\mathbf{L}\cdot\int\frac{d^2\mathbf{l}}{(2\pi)^2}\frac{C_l^{TT}\tilde{T}(\mathbf{l})\tilde{T}(\mathbf{L}-\mathbf{l})}{\tilde{C}_l^{tot}\tilde{C}^{tot}_{|\mathbf{l}-\mathbf{L}|}} \tag{4.34}$$

This has lowest order variance, or noise, given by

$$\delta(\mathbf{0})\langle|\hat{\psi}(\mathbf{L})|^2\rangle^{-1} = N(\mathbf{L})^{-1} = \int\frac{d^2\mathbf{l}}{(2\pi)^2}\frac{[(\mathbf{L}-\mathbf{l})\cdot\mathbf{L}C^{TT}_{|\mathbf{l}-\mathbf{L}|} + \mathbf{l}\cdot\mathbf{L}C_l^{TT}]^2}{2\tilde{C}_l^{tot}\tilde{C}^{tot}_{|\mathbf{l}-\mathbf{L}|}} \tag{4.35}$$

We have constructed the estimator from solely the temperature field here. The polarisation fields also provide useful information and one can construct a total of 6 minimum variance estimators out of the three fields: $\{TT, TE, TB, EE, EB, BB\}$, each with different normalisation and weight functions, which may be found in [36]. BB, under the null hypothesis of $r = 0$ has vanishing signal to noise so is not used. Given a sufficiently sensitive experiment the EB estimator turns out to have the best signal-to-noise, and permits mapping out to $l = 1000$. The reason is that that assuming $r = 0$, the unlensed B mode has no cosmic variance, while the lensed B mode peaks at relatively high l, due to the presence of the sine term in 4.27 - see figure 10. This gives a large number of small-scale coherence patches in the sky in polarization to exploit, though also requires a high instrument sensitivity to make best use of. If high l measurements are noise limited, as is the case for Planck polarisation data, the estimators perform similarly, and can be used either together with inverse variance weighting, or to cross check each other.

5 Probing Inflationary Physics

The B mode diagnostic is often termed to be a 'smoking gun' for inflation: if detected it would provide very strong evidence for its occurrence, and give us significant insight into its physics. In this section we begin by explaining why this first statement is true, and go on to discuss what additional constraining power a detection of primordial tensor like perturbations would provide.

5.1 Inflation Alternatives

It is still up for debate as to whether inflation actually occurred, and a fair evaluation as to the status of inflation requires consideration of alternatives. Our confidence in inflation is twofold: firstly observational data thus far has been entirely consistent with what we might expect inflation to produce, and secondly through the striking absence of compelling alternatives. While there do exist several other theories for the early universe in the literature, they all suffer serious problems. We make this concrete for the particular alternative of an *Ekpyrotic* cosomology here [2].

One key motivation for inflation was that it necessarily causes the comoving horizon to shrink, solving the horizon problem, a problem which any contender to inflation must also deal with. Accelerated expansion is not the only mechanism that can do this: the contracting phase before a Big Crunch does so equally well. While inflation achieves shrinking $(aH)^{-1}$ via $H \approx$ const and $a(t)$ exponentially increasing, ekpyrosis relies instead on a phase of slow contraction $a(t) \approx$ const and H^{-1} decreasing. This is followed by a bounce leading to the hot Big Bang and standard decelerating FLRW cosmology. Its cyclic extension involves our current expansion to be followed by a contracting ekpyrotic phase, leading to a new hot Big Bang phase, continuing ad infinitum.

It however has a major theoretical issue. For the contracting phase to smoothly connect to the expanding Big Bang evolution (i.e. for there to be a bounce) we require

$$2M_{\rm pl}^2\dot{H}^2 = -(\rho + P) > 0 \tag{5.1}$$

i.e. a violation of the null energy condition. This can be achieved at the level of an effective field theory, though so far has suffered major stability issues when attempts have been made to embed it in a UV complete theory.

It also has an observational issue. A simple model for the ekpyrotic cosmology is analogous to inflation, an effective theory of a scalar field, instead rolling fast down its potential. One expects therefore the curvature perturbation to have a very blue spectrum, in stark contrast with the observed near scale invariance. Similarly the tensor spectrum is highly blue, resulting in exponentially small IGW amplitudes for observable modes.

Both points turn out to be rather representative of alternatives to inflation. Other examples include String Gas Cosmology, or Pre-Big Bang Cosmology, both rooted in String Theory. These too suffer major theoretical issues, stemming from novel and not well understood physics, which require addressing before the models can be regarded as compelling alternatives to inflation. Furthermore, they often produce negligible primordial tensor perturbations. This strengthens the constraining power of the B mode diagnostic: a detection of primordial tensor perturbations has the power to rule out some of these other models completely and really does provide strong evidence for inflation.

5.2 Probes of Fundamental Physics

Inflation so far is an excellent phenomenological paradigm for the early universe, and so it is natural to inquire about the underlying theoretical structure. In particular, how do the scalar fields involved in inflation relate to other, better understood and well tested areas of physics. A true 'model of infation' is more than merely a choice of effective action for some scalar fields. It it is instead an answer to at least some of the following fundamental questions [2]:

1. Is the inflaton a particle we know about or is 'new physics' beyond the Standard Model or modified gravity at play?
2. How does the inflaton interact with the Standard Model? Inflation must eventually end and reheat the universe, creating all Standard Model particles, so it certainly must somehow.
3. What is the energy scale of inflation? How far does the inflaton field travel during inflation and what causes it to stop?
4. How many light degrees of freedom are relevant during inflation?

Theoretical physics has come a long way in mapping out a range of consistent and well-motivated inflationary mechanisms and their phenomenological predictions. However, theory alone may not distinguish between them all, and to answer these questions, some easier than others, there is a pressing need for observational data. Here we discuss the implications of a measurement of r, which may just be around the corner, on some of the above questions. We begin with some generic (SFSR) model independent results, and then discuss briefly what one can say about a given model.

In the slow roll approximation the tensor power spectrum depends only on the Hubble rate during inflation, while the scalar power spectrum depends additionally on the slow roll parameter ϵ. We may use $3H^2M_{\rm pl}^2 \approx V$ to rewrite the scalar and tensor power spectra 2.25 as

$$\begin{aligned} \Delta_s^2(k) &= \frac{V}{24\pi^2\epsilon M_{\rm pl}^4} \qquad n_s = 2\eta_V - 6\epsilon_V \\ \Delta_t^2(k) &= \frac{2V}{3\pi^2 M_{\rm pl}^4} \qquad n_t = -2\eta_V \qquad r = 16\epsilon_V \end{aligned} \tag{5.2}$$

Potential Shape

Recall $\epsilon_V = \epsilon_V(V, V')$ and $\eta_V = \eta_V(V, V'')$. Therefore measurements of $A_t \to V$, $A_s \to V'$ and $n_s \to V''$ at some pivot scale. We can go further by introducing the running of n_s, i.e. its scale dependence, which gives us V'''. From this we may reconstruct the inflaton potential as a taylor series around ϕ_*, corresponding to the time when fluctuations at the CMB pivot scale $k_* = 0.05 Mpc^{-1}$ exit the horizon

$$V(\phi) = V|_* + V'|_*(\phi - \phi_*) + \frac{1}{2}V''|_*(\phi - \phi_*)^2 + \frac{1}{3}V'''|_*(\phi - \phi_*)^3 + \dots \tag{5.3}$$

Energy Scale of Inflation

While we may compute this using just A_t, we may as well use A_s too. Using 5.2, $A_s \approx 2.2 \times 10^{-9}$, and $M_{\rm pl} \approx 2.43 \times 10^{18}$GeV we can write

$$\begin{aligned} V = 24\pi^2 A_s \frac{r}{16} M_{\rm pl}^4 \Rightarrow V^{1/4} &\approx 1.06 \times 10^{16}\text{GeV}\left(\frac{r_*}{0.01}\right)^{1/4} \\ &\leq 1.75 \times 10^{16}\text{GeV} \end{aligned} \tag{5.4}$$

where the inequality comes from the bound $r_* < 0.1$. A detectably large tensor amplitude would demonstrate a tremendously high new fundamental energy scale in physics - comparable to that of Grand Unified Theories. We will have unlocked a unique probe of an energy scale roughly 12 orders of magnitude higher than accessible in terrestrial collider experiments, a result exceedingly important for the high energy physics community.

Field Excursion

In the slow roll regime ϵ contains information about the background evolution of the field. In particular, recalling our previous calculation 2.12 we can compute the 'field excursion' of the inflaton field in Planck units

$$\begin{aligned} N(t) &= \int_{\phi(t)}^{\phi_{end}} \frac{d\phi}{\sqrt{2\epsilon}M_{\rm pl}} \\ \Rightarrow dN &= \frac{d\phi}{\sqrt{2\epsilon}M_{\rm pl}} \\ \Rightarrow \frac{\Delta\phi}{M_{\rm pl}} &= \int_0^N \sqrt{2\epsilon}dN = \int_0^N \sqrt{\frac{r}{8}}dN \end{aligned} \tag{5.5}$$

The total field excursion between the end of inflation and the time when fluctuations were created on CMB scales is then

$$\frac{\Delta\phi}{M_{\rm pl}} = \int_0^{N_*} \sqrt{\frac{r(N)}{8}}dN = \left(\frac{r_*}{8}\right)^{\frac{1}{2}} N_{\rm eff} \tag{5.6}$$

where $N_{\rm eff}$ is model dependent and given by

$$\int_0^{N_*} \left(\frac{r(N)}{r_*}\right)^{\frac{1}{2}} dN \tag{5.7}$$

In slow roll inflation r is approximately constant, depending slightly on N, precisely because ϵ varies slightly during inflation. r varies only at second order in slow roll parameters and we can estimate $N_{\rm eff} \approx 30 - 60$ to give

$$\frac{\Delta\phi}{M_{\rm pl}} > 1.06 \times \left(\frac{r_*}{0.01}\right)^{1/2} \tag{5.8}$$

where the inequality comes from a conservative lower limit on $N_{\rm eff} > 30$. We can see inflation models seperate into two (vaguely) distinct classes, depending on if $r \lessapprox 0.01$ or $r \gtrapprox 0.01$, known as small and large field models. This is the Lyth bound [38].

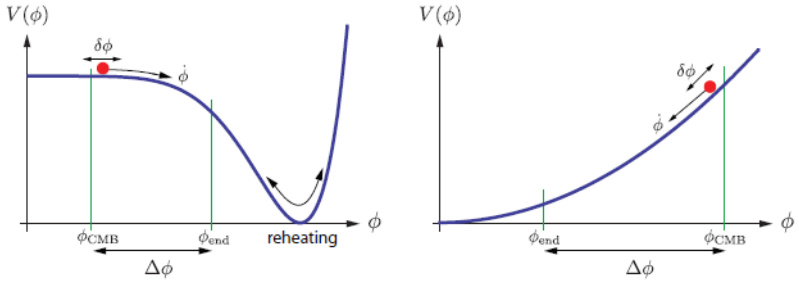

Figure 11. Examples of typical small (left) and large (right) field models, with field excursion shown. Figure taken from [39].

While both small and large field models are challenging to construct consistently, and require some degree of fine tuning, large field models prove more difficult. Suppose we expand the inflaton potential in an SFSR model as

$$V(\phi) = \frac{1}{2}m^2\phi^2 + \sum_{p=3}^{\infty} \lambda_p \left(\frac{\phi}{M_{\rm pl}}\right)^p \tag{5.9}$$

We can fine tune λ_p such that at any ϕ, $(\epsilon, \eta) \ll 1$, though these coefficients are expected to receive quantum corrections $\Delta\lambda_p(\phi)$, which generically will be of order unity in superPlanckian field ranges, expected in large field inflation. It is hard to see inflation being maintained for sufficiently many e

folds as $(\epsilon, \eta) \ll 1$ would likely not be preserved over this full range.

A detection (or lack thereof) of r in upcoming CMB experiments, with forecasted sensitivity $r \approx 10^{-3}$, would have far reaching implications for inflationary model building. It would be able to definitively either validate or rule out such large field models, and further would give information about the full UV completion of the inflaton field theory and gravity, and hence a clue towards quantum gravity.

5.3 Inflation Models

Having worked fairly model independently thus far, we give some examples of particular inflation models, and their general predictions for observables, focussing initially on SFSR. In this context, a model prescribes the potential V and a number of e folds of inflation N_* at some pivot scale, a kind of initial condition. From this, we may deduce two observational quantities of interest n_s and r. There exist many such models, here we'll just list a few.

We demonstrate the calculation alluded to above in the case of a simple large field power law model [13]

$$V(\phi) = \frac{1}{2} m^{4-\alpha} \phi^{\alpha} \tag{5.10}$$

for m a mass parameter required to give the potential the correct mass dimension. We may compute

$$\epsilon_V = \frac{M_{\rm pl}^2 \alpha^2}{2\phi^2} \tag{5.11}$$

and therefore

$$N = \int_{\phi_e}^{\phi} \frac{d\phi}{M_{\rm pl}} \frac{1}{\sqrt{2\epsilon}} = \frac{1}{2M_{\rm pl}^2}(\phi^2 - \phi_e^2) = \frac{\alpha}{4}\left(\frac{1}{\epsilon - 1}\right) \tag{5.12}$$

using $\epsilon(\phi_e) = 1$. This gives $\epsilon_V \approx \frac{\alpha}{4N}$. Using this, one calculates $\eta_V = \frac{\alpha - 1}{2N}$. Finally we obtain using 2.26

$$n_s - 1 = -\frac{2+\alpha}{2N} \qquad r = \frac{4\alpha}{N} \tag{5.13}$$

The hilltop model is a fairly typical looking small-field model, with

$$V(\phi) \propto 1 - \left(\frac{\phi}{\mu}\right)^p + \dots \tag{5.14}$$

for $p > 2$ and $\phi < \mu \ll M_{\rm pl}$ and may be considered as an approximation to a generic symmetry breaking potential, with the dots denoting higher order terms becoming important near the end of inflation and during reheating.

These parameters provide a simple way of meeting SFSR models with observational data, as demonstrated for the above models and many others in figure 12. In general SFSR models can have a blue or red tilt, with current measurements of the primordial scalar power ruling out all blue models. From the precise shape of the data we get more stringent constraints. For progress to be made we must further constrain the range of allowed r values - a detection of r to any uncertainty would do so significantly, collapsing the semicircular contour in the (n_s, r) plane into a tighter elliptical shape.

In this section we have only scratched the surface of the vast literature on inflationary models. We have worked only with SFSR models, though by taking a non trivial kinetic term in 2.5 one gets a more generic single field model. One can also add more effective fields, extending the number of possibilities massively though diminishing predictive power, to obtain a multifield model. We can develop further plausible models by introducing a non minimal coupling to gravity, or by modifying gravity entirely, though this last one is substantially harder to do consistently [39].

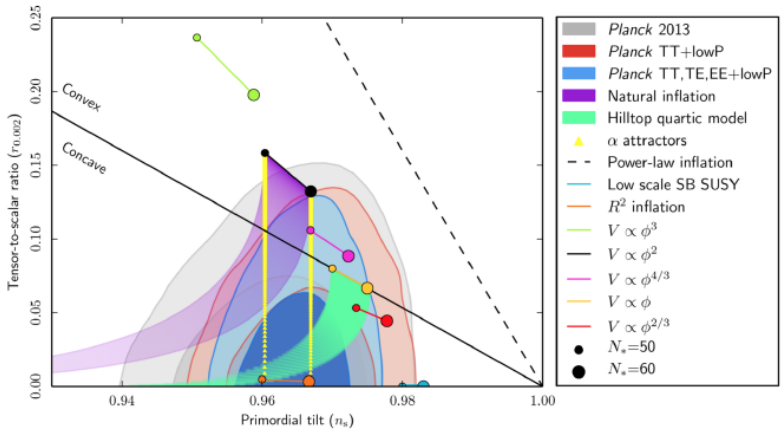

Figure 12. Constraints on n_s and r by iterations of Planck data releases, taken from [13]. The predictions for $N_* = 50$ and $N_* = 60$ from a variety of different inflationary models are shown. Concave and convex refer to the sign of the second derivative of the inflaton potential. 'lowP' refers to data from the large-scale WMAP polarization survey.

For illustration beyond SFSR, we describe briefly how we may be able to distinguish some of these classes of model by a measurement of the scale dependence of the tensor power spectrum. To see this, working through a similar calculation to ours, one finds for generic single field models the tensor to scalar ratio depends on the sound speed [2]

$$c_s^2 = \frac{P_{,X}}{\rho_X} = \frac{P_{,X}}{P_{,X} + 2XP_{,XX}} \tag{5.15}$$

leading to the prediction on the consistency relation $r = -8n_t$ being modified to

$$r = -8c_s n_t \tag{5.16}$$

providing an experimental test for non canonical physics. Multifield models enjoy a similar consistency relation

$$r = -8n_t \sin^2 \Delta \tag{5.17}$$

where $\sin^2 \Delta$ parametrises the ratio between the adiabatic scalar power spectrum at horizon exit during inflation and that which is observed today. In two field inflation this is directly measurable. These consistency criterion may be used as generic tests for broad families of inflation models, though do rely on a measurement of the scale dependence of tensor power spectrum n_t, which is still far in the future.

6 Prospects and Conclusion

The CMB has had a strong track-record of providing major breakthroughs in cosmology. Its first detection gave further independent evidence for the expansion of the universe, firmly shifting the community view from a 'steady state' universe towards the mostly correct Big Bang model described by an adiabatically expanding and cooling FLRW solution. Its small temperature anisotropies have given us incredibly precise measurements of certain important cosmological parameters over the past few decades. B modes from IGWs are the next frontier - a measurement of them would have far reaching consequences for cosmology as well as other areas of physics today. The challenge now is to make these measurements on which this entire essay is based. There exist no major cosmological issues in doing so; through decades of theoretical work we have a good quantitative understanding of the zoo of early and late universe effects that may contribute both to CMB temperature anisotropies and polarisation, up to some free parameters.

We can therefore attribute the lack of detection so far to two reasons. While we have a reasonable understanding of the theory of contaminants to the primary CMB, removing them to reveal the small inflationary B mode signal remains difficult. Over the last few years major advances have been made in the realms of foreground separation and delensing so these are slowly becoming manageable. Secondly, as is common with astrophysics, technological advances are necessary to drive progress. The CMB was predicted an entire 17 years before its first detection in 1965, and a further 25 years followed before COBE first measured its anisotropies in 1990. The roadblock was always technological, not that we did not appreciate the potential significance of these discoveries. To detect inflationary B modes we clearly require an even greater level of sensitivity and precision than was available in even the most recent generation of CMB experiments, and so more work needs to be done on the experimental side too.

Given the significance a detection would have, there is a massive global effort under way in attempting a measurement of B modes. If r is not too far below the current upper bound, which is certainly plausible given the vast array of well motivated inflationary models whose prediction for r lies in this large field regime, a detection may be just around the corner, in the next few years. Our best prospects for this are through complementing upcoming ground based experiments such as CMB-S4, with space based missions such as LiteBIRD, PIXIE or COrE [40]. Space based satellite or balloon missions have the advantage of little or no obscuring atmospheric noise, and wider possible sky coverage allowing access to low l modes, whereas ground based measurements will generally focus on smaller angular scales. CMB-S4 for example boasts a target sensitivity of $\sigma(r) \sim 10^{-3}$, through focussing on the degree scale recombination peak expected in the B mode spectrum.

If successful, we will unlock a new probe of fundamental physics at some of the highest energy scales expected in nature and earliest times we may expect to have access to. It will provide definitive proof of inflation, and would constrain its properties significantly. Further work into characterising this IGW signal through measurements of n_t and other parameters will provide us with further insights. The far reaching consequences of this make the considerable effort being put into detecting these inflationary B modes completely worth it, despite our lack of success so far. Even if unsuccesful, this effort is not in vain - a lack of detection to high sensitivity, while not giving concrete evidence for inflation, would still significantly constrain it. Furthermore, the inflationary epoch is not the sole goal of CMB science right now, and so much of this work carries over to other important science goals such as better constraining neutrino physics, dark matter, and dark energy [40].

A SFSR Power Spectra Derivation

We derive here the relevant power spectra in SFSR for scalar and tensor perturbations.

A.1 Scalars

In spatially flat gauge, perturbations to ζ are related to those of the inflation field $\delta\phi$ via 2.16

$$\zeta = -\frac{\mathcal{H}}{\bar{\phi}'}\delta\phi \tag{A.1}$$

where the bar denotes the homogeneous background, since the inflation is the dominant energy source and $\Psi = 0$. We have switched to conformal time. Therefore

$$\Delta_s^2(k) = \left(\frac{\mathcal{H}}{\bar{\phi}'}\right)^2 \Delta_{\delta\phi}^2(k) \tag{A.2}$$

To compute the $\delta\phi$ power spectrum, we must quantise the inflaton, and briefly review how we do so here, over a quasi-de Sitter background, following [4]. We work in conformal time, and the equations of motion simplify if we introduce a related field f

$$\delta\phi(\tau, \mathbf{x}) = \frac{f(\tau, \mathbf{x})}{a(\tau)} \tag{A.3}$$

We begin with the action for the inflaton

$$S = \int d\tau d^3x \sqrt{-g}\left(-\frac{1}{2}g^{\mu\nu}\partial_\mu\phi\partial_\nu\phi - V(\phi)\right) \tag{A.4}$$

We may take the metric to be the unperturbed FLRW metric here since interactions arising form perturbations to $g_{\mu\nu}$ are slow roll suppressed [3]. Plugging in the unperturbed FLRW metric we get

$$S = \int d\tau d^3x \left(\frac{1}{2}a^2[(\phi')^2 - (\nabla\phi)^2] - a^4V(\phi)\right) \tag{A.5}$$

We now plug in A.3 and expand. The first order piece just gives the Klein Gordon for the background field (in conformal time), as expected. The second order piece gives

$$S^{(2)} = \frac{1}{2}\int d\tau d^3x \left((f')^2 - (\nabla f)^2 + (\frac{a''}{a} - a^2V'')f^2\right) \tag{A.6}$$

after integrating by parts and making use of F2 in conformal time. In the slow roll approximation we may drop the potential term since it is slow roll suppressed compared to the other terms. So the second order action is

$$S^{(2)} \approx \frac{1}{2}\int d\tau d^3x \left((f')^2 - (\nabla f)^2 + \frac{a''}{a}f^2\right) \tag{A.7}$$

Note since we have dropped the potential entirely, this is just the second order action for a free massless scalar field. Integrating by parts and demanding $S^{(2)} = 0$ gives the Muhkanov Sasaki equation, which we can write in real or Fourier space

$$\begin{aligned} & f'' - \nabla^2 f - \frac{a''}{a}f = 0 \\ \Leftrightarrow \quad & f_{\mathbf{k}}'' + (k^2 - \frac{a''}{a})f_{\mathbf{k}} = 0 \end{aligned} \tag{A.8}$$

We treat these perturbations f quantum mechanically. We'll outline the key steps in quantising this system.

The conjugate momentum to f is $\pi(\tau, \mathbf{x}) = \frac{\partial \mathcal{L}}{\partial f'} = f'$ using A.5. We promote these to operators $\hat{f}(\tau, \mathbf{x})$ and $\hat{\pi}(\tau, \mathbf{x})$ satisfying equal time commutation relations which read in real and Fourier space

$$\begin{aligned} [\hat{f}(\tau, \mathbf{x}), \hat{\pi}(\tau, \mathbf{x}')] &= i\delta(\mathbf{x} - \mathbf{x}') \\ [\hat{f}_{\mathbf{k}}(\tau), \hat{\pi}_{\mathbf{k}'}(\tau)] &= (2\pi)^3 \delta(\mathbf{k} + \mathbf{k}') \end{aligned} \tag{A.9}$$

We mode expand $\hat{f}_{\mathbf{k}}(\tau) = f_k(\tau)\hat{a}_{\mathbf{k}} + f_k^*(\tau)\hat{a}_{\mathbf{k}}^\dagger$, demanding the modefunctions $f_k(\tau)$ and $f_k^*(\tau)$ to be two linearly independent solutions of the Muhkanov-Sasaki equation. Substituting into the commutation relations we get

$$W[f_k, f_k^*] \times [\hat{a}_{\mathbf{k}}, \hat{a}_{\mathbf{k}'}^\dagger] = (2\pi)^3 \delta(\mathbf{k} + \mathbf{k}') \tag{A.10}$$

which after normalising the Wronskian to 1 gives the usual commutator of annhilation and creation operators

$$[\hat{a}_{\mathbf{k}}, \hat{a}_{\mathbf{k}'}^\dagger] = (2\pi)^3 \delta(\mathbf{k} + \mathbf{k}') \tag{A.11}$$

We can now define the Hilbert space as the usual Fock space formed by unions of n particle states obtained by applying n creation operators to the the vacuum, satisfying

$$\hat{a}_{\mathbf{k}}|0\rangle = 0 \qquad \forall \mathbf{k} \tag{A.12}$$

Note this doesn't completely fix the vacuum, since we have not yet fixed our mode functions. We construct the Bunch-Davies vacuum, by imposing the mode functions must be positive frequency and match the minkowski mode functions $f_k(\tau) \propto e^{\pm ik\tau}$ at early times, since at early times $\tau \to -\infty$ the Muhkanov Sasaki equation A.8 reduces to

$$f_{\mathbf{k}}'' + k^2 f_{\mathbf{k}} = 0 \tag{A.13}$$

Now we make use of the quasi-de Sitter approximation, where H is constant and $a = -\frac{1}{H\tau}$, and so A.8 becomes

$$f_k'' + (k^2 - \frac{2}{\tau^2}) f_k = 0 \tag{A.14}$$

with general solution

$$f_k(\tau) = \alpha \frac{e^{-ik\tau}}{\sqrt{2k}} \left(1 - \frac{i}{k\tau}\right) + \beta \frac{e^{ik\tau}}{\sqrt{2k}} \left(1 + \frac{i}{k\tau}\right) \tag{A.15}$$

which matches our initial condition for $\beta = 0$ and $\alpha = 1$, giving the Bunch Davies mode function

$$f_k(\tau) = \frac{e^{-ik\tau}}{\sqrt{2k}} \left(1 - \frac{i}{k\tau}\right) \tag{A.16}$$

Finally we may compute the power spectrum of $\delta\phi$. The power spectrum of the f field is computed easily as

$$\begin{aligned} \langle f_{\mathbf{k}} f_{\mathbf{k}'} \rangle &= \langle 0 | (f_k(\tau)\hat{a}_{\mathbf{k}} + f_k^*(\tau)\hat{a}_{\mathbf{k}}^\dagger)(f_k(\tau)\hat{a}_{\mathbf{k}'} + f_k^*(\tau)\hat{a}_{\mathbf{k}'}^\dagger)|0\rangle \\ &= (2\pi)^3 \delta(\mathbf{k} - \mathbf{k}')|f_k(\tau)|^2 \end{aligned} \tag{A.17}$$

and so the dimensionless power spectra of interest is

$$\begin{aligned} \Delta^2_{\delta\phi}(k) &= \frac{1}{a^2}\Delta^2_f(k) \\ &= \frac{k^3}{2\pi^2 a^2}|f_k|^2 \\ &= \frac{k^2}{4\pi^2 a^2}\left(1 + \frac{1}{k^2\tau^2}\right) \\ &= \left(\frac{H}{2\pi}\right)^2 \left(1 + \frac{k^2}{a^2 H^2}\right) \quad \text{using } a = -\frac{1}{H\tau} \end{aligned} \tag{A.18}$$

We evaluate the power spectrum at horizon crossing, when the modes become superhorizon and freeze out, to be

$$\Delta^2_{\delta\phi}(k) \approx (\frac{H}{2\pi})^2|_{k=aH} \tag{A.19}$$

and so, making use of 2.3

$$\begin{aligned}\Delta^2_s(k) &= \left(\frac{\mathcal{H}}{\bar{\phi}'}\right)^2 \Delta^2_{\delta\phi}(k) \\ &= \frac{1}{2\epsilon M^2_{\rm pl}}\left(\frac{H}{2\pi}\right)^2|_{k=aH}\end{aligned} \tag{A.20}$$

A.2 Tensors

In the previous section we used gauge freedom to avoid quantising the metric directly, though for tensor perturbations we are forced to. We isolate the the tensor perturbations as

$$ds^2 = a^2(\tau)[-d\tau^2 + (\delta_{ij} + \xi_{ij})dx^i dx^j] \tag{A.21}$$

where ξ_{ij} is symmetric, transverse, and traceless: ie $\xi_{ij} = \xi_{ji}$, $\partial_i \xi_{ij} = 0$ and $\xi_{ii} = 0$.

We expand the full action to second order in ξ, using the Friedmann equations. This calculation is rather long, so we omit the details here, but one can find them at [41].

$$S = \int d\tau d^3x\sqrt{-g}\left(\frac{M^2_{\rm pl}}{2}R + \mathcal{L}_\phi\right) \to S^{(2)} = \frac{M^2_{\rm pl}}{8}\int d\tau d^3x[\xi'_{ij}\xi'_{ij} - \partial_k\xi_{ij}\partial_k\xi_{ij}] \tag{A.22}$$

By rotation symettry of the problem these are the only terms we expect to appear at second order, though one has to go through the calculation to get the correct numerical factors as they turn out to be important. We may expand this graviton into its two polarisation states and as plane waves [3]

$$\xi_{ij}(\tau, \mathbf{x}) = \int \frac{d^3\mathbf{k}}{(2\pi)^3}\sum_{s=+,x}\epsilon^s_{ij}(\mathbf{k})\xi_s(\tau, \mathbf{k})e^{i\mathbf{k}\cdot\mathbf{x}} \tag{A.23}$$

where ϵ^s_{ij} are in general complex polarisation tensors satisfying

$$\epsilon^s_{ii}(\mathbf{k}) = k^i\epsilon^s_{ij}(\mathbf{k}) = 0 \qquad \text{transverse and traceless} \tag{A.24}$$

$$\epsilon^s_{ij}(\mathbf{k}) = \epsilon^s_{ji}(\mathbf{k}) \qquad \text{symettric} \tag{A.25}$$

$$\epsilon^s_{ij}(\mathbf{k})\epsilon^s_{jk}(\mathbf{k}) = 0 \qquad \text{null} \tag{A.26}$$

$$\epsilon^s_{ij}(\mathbf{k})\epsilon^s_{ij}(\mathbf{k})^* = 2\delta_{ss'} \qquad \text{normalisation} \tag{A.27}$$

$$\epsilon^s_{ij}(\mathbf{k})^* = \epsilon^s_{ij}(-\mathbf{k}) \qquad \xi_{ij} \text{ real} \tag{A.28}$$

For a fixed wavevector $\mathbf{k}$ we may choose a particular basis of simple polarisation tensors to simplify calculations, and do so in 3.2. Inserting this expansion into $S^{(2)}$ we obtain

$$S^{(2)} = \frac{M^2_{\rm pl}}{2}\frac{1}{2}\int\frac{d^3\mathbf{k}}{(2\pi)^3}d\tau a^2\sum_{s=+,x}\xi'_s(\tau, \mathbf{k})\xi'_s(\tau, -\mathbf{k}) - k^2\xi_s(\tau, \mathbf{k})\xi_s(\tau, -\mathbf{k}) \tag{A.29}$$

This, up to a constant, is really just two copies of a special case of the the second order action for the inflaton A.5. To see this, consider writing A.5 in Fourier space $\phi(\mathbf{x}) = \int\frac{d^3\mathbf{k}}{(2\pi)^3}\phi(\mathbf{k})e^{i\mathbf{k}\cdot\mathbf{x}}$ for the case where $\bar{\phi} = V(\bar{\phi}) = 0$, i.e. $\phi = \delta\phi$

$$\begin{aligned}S^{(2)} &= \frac{1}{2}\int d\tau d^3x a^2[(\phi')^2 - (\nabla\phi)^2] \\ &= \frac{1}{2}\int\frac{d^3\mathbf{k}}{(2\pi)^3}d\tau a^2[\phi'(\tau, \mathbf{k})\phi'(\tau, -\mathbf{k}) - k^2\phi(\tau, \mathbf{k})\phi(\tau, -\mathbf{k})]\end{aligned} \tag{A.30}$$

We may therefore quantise the two independent fields $\tilde{\xi_s} = \frac{M_{\rm pl}a}{\sqrt{2}}\xi_s$ exactly as we did $f = a\delta\phi$, noting they obey the same Muhkanov-Sasaki equation A.8 as in the scalar case. The normalisation is required to give canonical factor of $\frac{1}{2}$ on the kinetic term in the action, which plays a role when we fix the Wronskian to 1. Going through the same procedure as before, we get

1. Operators $\hat{\xi}_s(\mathbf{k}) = \frac{\sqrt{2}}{M_{\rm pl}a}(f_k\hat{a}_{\mathbf{k}s} + f_k^*\hat{a}^\dagger_{\mathbf{k}s})$
2. Commutation relations $[\hat{a}_{\mathbf{k}s}, \hat{a}^\dagger_{\mathbf{k}'s'}] = (2\pi)^3\delta(\mathbf{k}+\mathbf{k}')\delta_{ss'}$
3. The same Bunch-Davies mode functions $f_k(\tau)$

The final result of this section is to calculate the tensor power spectrum. We have

$$\begin{aligned}\langle\xi_{ij}(\mathbf{k})\xi_{ij}(\mathbf{k}')\rangle &= \sum_{ss'}\epsilon^s_{ij}(\mathbf{k})\epsilon^s_{ij}(\mathbf{k}')\langle\xi_s(\mathbf{k})\xi_s(\mathbf{k}')\rangle \\ &= \left(\frac{\sqrt{2}}{M_{\rm pl}a}\right)^2\sum_{ss'}\epsilon^s_{ij}(\mathbf{k})\epsilon^s_{ij}(\mathbf{k}')(2\pi)^3\delta(\mathbf{k}+\mathbf{k}')|f_k|^2 \\ &= \left(\frac{\sqrt{2}}{M_{\rm pl}a}\right)^2\sum_{ss'}2\delta_{ss'}(2\pi)^3\delta(\mathbf{k}+\mathbf{k}')|f_k|^2 \\ &= (2\pi)^3\delta(\mathbf{k}+\mathbf{k}')\frac{8}{M_{\rm pl}^2a^2}|f_k|^2\end{aligned} \tag{A.31}$$

using several of the properties A.25-A.28. We can read off

$$\Delta^2_t(k) = \frac{8}{M_{\rm pl}^2}\Delta^2_{\delta\phi}(k) = \frac{2}{\pi^2}\left(\frac{H}{M_{\rm pl}}\right)^2|_{k=aH} \tag{A.32}$$

evaluated again at horizon exit, after which the modes become superhorizon and freeze out. We discuss their evolution after horizon reentry in 3.3.1.

B Properties of Spin-Weighted Functions

We list here the properties of spin-weighted functions we'll need [12]. For each integer spin s separately, there exists a basis of spin-weighted functions ${}_sY_{lm}$ on the sphere, satisfying the same orthogonality and completeness relations as regular spherical harmonics

$$\begin{aligned}\int_0^{2\pi}d\phi\int_{-1}^{1}d(\cos\theta)\,{}_sY_{lm}(\theta,\phi)\,{}_sY^*_{l'm'}(\theta,\phi) = \delta_{ll'}\delta_{mm'} \\ \sum_{lm}{}_sY^*_{lm}(\theta,\phi)\,{}_sY_{lm}(\theta',\phi') = \delta(\phi-\phi')\delta(\theta-\theta')\end{aligned} \tag{B.1}$$

There also exist spin raising ($\eth$) and spin lowering ($\bar{\eth}$) operators, which raise or lower the spin weight of a function ${}_sf(\theta,\phi)$ by 1, with explicit expressions given by

$$\begin{aligned}\eth_s f(\theta,\phi) &= -\sin^s\theta[\partial_\theta + i\csc\theta\partial_\phi]\sin^{-s}\theta\,{}_sf(\theta,\phi) \\ \bar{\eth}_s f(\theta,\phi) &= -\sin^{-s}\theta[\partial_\theta - i\csc\theta\partial_\phi]\sin^{s}\theta\,{}_sf(\theta,\phi)\end{aligned} \tag{B.2}$$

Polarisation quantities are spin ±2, which we often wish to raise or lower to spin 0. Suppose we have ${}_{\pm2}f(\mu,\phi)$ satisfying $\partial_\phi f = imf$. Acting twice with spin raising or lowering operators gives

$$\begin{aligned}\eth^2{}_{-2}f(\mu,\phi) &= (-\partial_\mu - \frac{m}{1-\mu^2})^2[(1-\mu^2){}_{-2}f(\mu,\phi)] \\ \bar{\eth}^2{}_2f(\mu,\phi) &= (-\partial_\mu + \frac{m}{1+\mu^2})^2[(1-\mu^2){}_2f(\mu,\phi)]\end{aligned} \tag{B.3}$$

where $\mu = \cos\theta$. The spin weighted spherical harmonics ${}_sY_{lm}$ are related to the standard spherical harmonics Y_{lm} by the relations

$$ {}_sY_{lm} = \begin{cases} [\frac{(l-s)!}{(l+s)!}]^{1/2} \eth^s Y_{lm} & 0 \leq s \leq l \\ [\frac{(l-s)!}{(l+s)!}]^{1/2} (-1)^s \bar{\eth}^s Y_{lm} & -l \leq s \leq 0 \end{cases} \tag{B.4} $$

derived using some of the following useful identities

$$ \begin{aligned} {}_sY^*_{lm} &= (-1)^s {}_{-s}Y_{l,-m} \\ \eth_s Y_{lm} &= \sqrt{(l-s)(l+s+1)}\,{}_{s+1}Y_{l,m} \\ \bar{\eth}_s Y_{lm} &= \sqrt{(l-s)(l-s+1)}\,{}_{s-1}Y_{l,m} \\ \bar{\eth}\eth_s Y_{lm} &= -(l-s)(l+s+1)\,{}_sY_{l,m} \end{aligned} \tag{B.5} $$

C Essay Description

Our most promising theory for the early universe involves a phase of cosmic inflation, which not only rapidly expands and flattens the universe, but also generates the primordial density perturbations from quantum fluctuations in the inflaton field. While we have good evidence for inflation, e.g. from the Gaussianity, adiabaticity and near-scale invariance of the scalar density perturbations, one prediction of inflation has not yet been found: many inflationary models produce a stochastic background of primordial gravitational waves. A detection of this background would not only provide a definitive confirmation of inflation, but could also give new insights into the microphysics of inflation and, more broadly, physics at the highest energies.

The best current way of finding this gravitational wave background is to search for a characteristic pattern in the polarization of the Cosmic Microwave Background (CMB), the B mode polarization. This essay should explain the physics underlying the search for this B mode polarization pattern, which is currently a major area of research in cosmology. The essay should first review the calculation of the gravitational wave background produced by standard single-field slow-roll inflation, a standard result described in past Part III lecture notes as well as a comprehensive review of the field [13]. The essay should also explain why the strength of the gravitational wave background (together with the scalar spectral index) can provide powerful constraints on the properties of inflation, such as the potential shape, energy scale, and field excursion [13, 40].

Drawing on [13, 40], past lecture notes and other resources, the essay should provide a (brief) review of the basics of CMB polarization, describe what the CMB B mode polarization is, and explain why it is a powerful probe of inflationary gravitational waves.

The remaining parts of the essay can, to some extent, be tailored to the student's interests. One option is to explain in detail the major observational challenges in B mode searches for inflationary gravitational waves, discussing the problems of foregrounds (Bicep/Keck/Planck 2015) and gravitational lensing as well as mitigation methods such as multifrequency cleaning and delensing [42]. Another option is to focus more on the theoretical background, describing in detail different classes of inflationary models and what these generically predict for B mode polarization ([40] and references therein). Students may also discuss a combination of both observational and theoretical aspects.

Relevant Courses

Essential: Cosmology

Useful: Advanced Cosmology, Quantum Field Theory, General Relativity

References

[1] Guth AH. 1981 Inflationary universe: A possible solution to the horizon and flatness problems. *Physical Review D* **23**, 2, 347–356. (doi:10.1103/PhysRevD.23.347).

[2] Baumann D, et al. 2009 CMBPol Mission Concept Study: Probing Inflation with CMB Polarization. *AIP Conference Proceedings* pp. 10–120. (doi:10.1063/1.3160885).

[3] Pajer E. 2021. Part III Field Theory in Cosmology Lecture Notes. (available on moodle).

[4] Baumann D. 2021. Part III Cosmology Lecture Notes. (http://cosmology.amsterdam/education/cosmology/).

[5] Planck Collaboration, et al. 2020 Planck 2018 results. VI. Cosmological parameters. *Astronomy & Astrophysics* **641**, A6. (doi:10.1051/0004-6361/201833910).

[6] Planck Collaboration, et al. 2020 Planck 2018 results - X. Constraints on inflation. *Astronomy & Astrophysics* **641**, A10. (doi:10.1051/0004-6361/201833887).

[7] Hu W, White M. 1997 A CMB Polarization Primer. *New Astronomy* **2**, 4, 323–344. (doi:10.1016/S1384-1076(97)00022-5).

[8] Baldauf T. 2021. Part III Field Theory in Cosmology Lecture Notes. (http://www.damtp.cam.ac.uk/user/tb561/AdvCosmo/).

[9] Lewis A, Challinor A. 2006 Weak Gravitational Lensing of the CMB. *Physics Reports* **429**, 1, 1–65. (doi:10.1016/j.physrep.2006.03.002).

[10] Kosowsky A. 1996 Cosmic Microwave Background Polarization. *Annals of Physics* **246**, 1, 49–85. (doi:10.1006/aphy.1996.0020).

[11] Challinor A, Peiris H. 2009 Lecture notes on the physics of cosmic microwave background anisotropies. *AIP Conference Proceedings* **1132**, 1, 86–140. (doi:10.1063/1.3151849).

[12] Zaldarriaga M, Seljak U. 1997 All-sky analysis of polarization in the microwave background. *Physical Review D* **55**, 4, 1830–1840. (doi:10.1103/PhysRevD.55.1830).

[13] Kamionkowski M, Kovetz ED. 2016 The Quest for B Modes from Inflationary Gravitational Waves. *Annual Review of Astronomy and Astrophysics* **54**, 1, 227–269. (doi:10.1146/annurev-astro-081915-023433).

[14] Polnarev AG. 1985 Polarization and Anisotropy Induced in the Microwave Background by Cosmological Gravitational Waves. *Soviet Astronomy* **29**, 607–613.

[15] Pritchard JR, Kamionkowski M. 2005 Cosmic Microwave Background Fluctuations from Gravitational Waves: An Analytic Approach. *Annals of Physics* **318**, 1, 2–36. (doi:10.1016/j.aop.2005.03.005).

[16] Seljak U, Zaldarriaga M. 1996 A Line of Sight Approach to Cosmic Microwave Background Anisotropies. *The Astrophysical Journal* **469**, 437. (doi:10.1086/177793).

[17] Giannantonio T, Crittenden R. 2007 The effect of reionization on the cosmic microwave background–density correlation. *Monthly Notices of the Royal Astronomical Society* **381**, 2, 819–826. (doi:10.1111/j.1365-2966.2007.12282.x).

[18] Zhao W, Zhang Y. 2006 Analytic approach to the CMB polarization generated by relic gravitational waves. *Physical Review D* **74**, 083006. (doi:10.1103/PhysRevD.74.083006).

[19] Zaldarriaga M. 1997 Polarization of the Microwave Background in Reionized Models. *Physical Review D* **55**, 4, 1822–1829. (doi:10.1103/PhysRevD.55.1822).

[20] Kamionkowski M, Kosowsky A, Stebbins A. 1996 A Probe of Primordial Gravity Waves and Vorticity. *arXiv:astro-ph/9609132* (doi:10.1103/PhysRevLett.78.2058).

[21] Seljak U, Zaldarriaga M. 1997 Signature of gravity waves in the polarization of the microwave background. *Physical Review Letters* **78**, 11, 2054–2057. (doi:10.1103/physrevlett.78.2054).

[22] 2014. Scientists find 'smoking gun' evidence from the creation of the universe. (https://www.pbs.org/newshour/science/scientists-find-smoking-gun-big-bang).

[23] Lizarraga J, Urrestilla J, Daverio D, Hindmarsh M, Kunz M, Liddle AR. 2014 Constraining topological defects with temperature and polarization anisotropies. *Physical Review D* **90**, 10, 103504. (doi:10.1103/PhysRevD.90.103504).

[24] Sun S. 2017 Inflationary electroweak/particle phase transitions and new classical gravitational waves on CMB. *Everything about Gravity* pp. 168–174. (doi:10.1142/9789813203952_0019).

[25] Pogosian L, Vachaspati T, Yadav A. 2013 Primordial Magnetism in CMB B-modes. *Canadian Journal of Physics* **91**, 6, 451–454. (doi:10.1139/cjp-2012-0401).

[26] Caimapo CEH. 2018. PhD Thesis. (https://www.escholar.manchester.ac.uk/jrul/item/?pid=uk-ac-man-scw:315590).

[27] Samtleben D, Staggs S, Winstein B. 2007 The Cosmic Microwave Background for Pedestrians: A Review for Particle and Nuclear Physicists. *Annual Review of Nuclear and Particle Science* **57**, 1, 245–283. (doi:10.1146/annurev.nucl.54.070103.181232).

[28] Planck Collaboration, et al. 2016 *Planck* 2015 results: X. Diffuse component separation: Foreground maps. *Astronomy & Astrophysics* **594**, A10. (doi:10.1051/0004-6361/201525967).

[29] Delabrouille J, Cardoso JF, Jeune ML, Betoule M, Fay G, Guilloux F. 2009 A full sky, low foreground, high resolution CMB map from WMAP. *Astronomy & Astrophysics* **493**, 3, 835–857. (doi:10.1051/0004-6361:200810514).

[30] BICEP2 Colloboration, et al. 2014 BICEP2 I: Detection Of B-mode Polarization at Degree Angular Scales. *Physical Review Letters* **112**, 24, 241101. (doi:10.1103/PhysRevLett.112.241101).

[31] BICEP2/Keck and Planck Collaborations, et al. 2015 Joint Analysis of BICEP2/Keck Array and Planck Data. *Physical Review Letters* **114**, 10, 101301. (doi:10.1103/PhysRevLett.114.101301).

[32] Blanton MR, et al. 2017 Sloan Digital Sky Survey IV: Mapping the Milky Way, Nearby Galaxies, and the Distant Universe. *The Astronomical Journal* **154**, 28. (doi:10.3847/1538-3881/aa7567).

[33] Lewis A, Challinor A. 2000. CAMB. (https://camb.info/).

[34] POLARBEAR Collaboration, et al. 2014 A Measurement of the Cosmic Microwave Background B-Mode Polarization Power Spectrum at Sub-Degree Scales with POLARBEAR. *The Astrophysical Journal* **794**, 2, 171. (doi:10.1088/0004-637X/794/2/171).

[35] Sherwin BD, Schmittfull M. 2015 Delensing the CMB with the Cosmic Infrared Background. *Physical Review D* **92**, 4, 043005. (doi:10.1103/PhysRevD.92.043005).

[36] Hu W, Okamoto T. 2002 Mass Reconstruction with CMB Polarization. *The Astrophysical Journal* **574**, 2, 566–574. (doi:10.1086/341110).

[37] Darwish O, et al. 2020 The Atacama Cosmology Telescope: A CMB lensing mass map over 2100 square degrees of sky and its cross-correlation with BOSS-CMASS galaxies. *Monthly Notices of the Royal Astronomical Society* **500**, 2, 2250–2263. (doi:10.1093/mnras/staa3438).

[38] Lyth DH. 1997 What would we learn by detecting a gravitational wave signal in the cosmic microwave background anisotropy? *Physical Review Letters* **78**, 10, 1861–1863. (doi:10.1103/PhysRevLett.78.1861).

[39] Baumann D. 2012 TASI Lectures on Inflation. *(arXiv:0907.5424)* .

[40] Abazajian KN, et al. 2016 CMB-S4 Science Book, First Edition. *(arXiv:1610.02743)* .

[41] Wang M. 2018. Second Order Action for Gravitational Waves from Inflation. (http://www.icg.port.ac.uk/∼mikewang).

[42] Smith KM, Hanson D, LoVerde M, Hirata CM, Zahn O. 2012 Delensing cmb polarization with external datasets. *Journal of Cosmology and Astroparticle Physics* **2012**, 06, 014–014. (doi:10.1088/1475-7516/2012/06/014).